The vibrational energies of ozone up to the dissociation threshold: Dynamics calculations on an accurate potential energy surface

Rüdiger Siebert, Paul Fleurat-Lessard, and Reinhard Schinke
Max-Planck-Institut für Strömungsforschung, D-37073 Göttingen, Germany

Martina Bittererová
Slovak University of Technology, Department of Physical Chemistry, SK-81237 Bratislava, Slovak Republic

S. C. Farantos
Institute of Electronic Structure and Laser Foundation for Research and Technology-Hellas, and Department of Chemistry, University of Crete, Iraklion 711 10, Crete, Greece

(Received 23 January 2002; accepted 6 March 2002)

We present an *ab initio* potential energy surface for the ground electronic state of ozone. It is *global*, i.e., it covers the three identical C_{2v} (open) minima, the D_{3h} (ring) minimum, as well as the $O(^3P)+O_2(^3\Sigma_g^-)$ dissociation threshold. The electronic structure calculations are performed at the multireference configuration interaction level with complete active space self-consistent-field reference functions and correlation consistent polarized quadruple zeta atomic basis functions. Two of the O–O bond distances, R_1 and R_2, and the O–O–O bending angle are varied on a regular grid (ca. 5000 points with $R_1 \geqslant R_2$). An analytical representation is obtained by a three-dimensional cubic spline. The calculated potential energy surface has a tiny dissociation barrier and a shallow van der Waals minimum in the exit channel. The ring minimum is separated from the three open minima by a high potential barrier and therefore presumably does not influence the low-temperature kinetics. The dissociation energy is reproduced up to 90% of the experimental value. All bound states of nonrotating ozone up to more than 99% of the dissociation energy are calculated using the filter diagonalization technique and employing Jacobi coordinates. The three lowest transition energies for $^{16}O_3$ are 1101.9 cm^{-1} (1103.14 cm^{-1}), 698.5 cm^{-1} (700.93 cm^{-1}), and 1043.9 cm^{-1} (1042.14 cm^{-1}) for the symmetric stretch, the bending, and the antisymmetric stretch modes, respectively; the numbers in parentheses are the experimental values. The root-mean-square error for all measured transition energies for $^{16}O_3$ is only 5 cm^{-1}. The comparison is equally favorable for all other isotopomers, for which experimental frequencies are available. The assignment is made in terms of normal modes, despite the observation that with increasing energy an increasing number of states acquires local-mode character. At energies close to the threshold a large fraction of states is still unambiguously assignable, particularly those of the overtone progressions. This is in accord with the existence of stable classical periodic orbits up to very high energies. © *2002 American Institute of Physics.* [DOI: 10.1063/1.1473664]

I. INTRODUCTION

The kinetics of ozone formation and ozone dissociation is of great importance for the chemistry of the atmosphere.[1–3] Despite this importance there are still a number of fundamental questions, for which convincing answers are still due. For example, the temperature and pressure dependence of ozone formation rates shows unusual behaviors,[4] which are not understood even one decade after the measurements. As surmised by Hippler *et al.*[4] some of the effects may be attributed to long-lived metastable states, belonging either to low-lying electronic states or to the ground electronic state. Another problem, which is strongly related to the recombination of ozone, has especially puzzled researchers over many years: the unusually high enrichment in most of the heavy isotopomers of ozone.[5] This effect has been observed in tropospheric[6,7] and in stratospheric[8] ozone. It also has been investigated in numerous laboratory experiments.[9–12] For a recent review of isotope effects see Ref. 13. A third question concerns the temperature dependence of the rate of the $^{18}O+^{16}O_2 \rightarrow ^{16}O+^{16}O^{18}O$ exchange reaction. In a recent experimental study Wiegell *et al.*[14] deduced a negative temperature dependence, i.e., the thermal exchange rate *decreases* by about a factor of 2 from 140 K to 300 K.

In a series of theoretical studies, all based on transition-state theory, Marcus and collaborators investigated in detail the kinetics of ozone formation and dissociation.[15–18] Using a few parameters adjusted to reproduce some of the experimental results, they could reproduce an impressively large body of experimental data. This success seems to strongly indicate that most of the puzzles have been resolved. However, up to now the applicability of statistical models (RRKM theory) has not been confirmed—at least not on the basis of rigorous dynamics calculations. The density of states of ozone near the dissociation threshold is very small for a triatomic molecule consisting of three heavy atoms ($\rho \approx 0.07/cm^{-1}$ for $J=0$, Ref. 19). This and the observation that

a large number of bound as well as resonance states near the threshold can be unambiguously assigned in terms of three quantum numbers[19] make one wonder whether the basic assumption of all statistical theories—the rate for internal energy transfer is much larger than the dissociation rate of the activated O_3 complex[20]—is fulfilled.

The basis for rigorous spectroscopic, reactive, or dissociation calculations is an accurate and global potential energy surface (PES), which encompasses the entire accessible configuration space, from the bottom of the potential well to the dissociation threshold and above.[21] Because of the notorious difficulties encountered in electronic structure calculations for ozone, even for the lowest state (see below), the construction of an accurate global PES is a formidable task.

The electronic structure of the low-lying states of ozone have been investigated by many authors (see Refs. 22–27 and references therein). Up to now there is only one global PES for $O_3(\tilde{X})$, which has been calculated by *ab initio* methods.[28] It had been constructed in order to define initial wave packets in the UV photodissociation of ozone rather than studying dissociation in the ground electronic state. The PES of Yamashita *et al.*[28] has been empirically modified by eliminating a relatively high dissociation barrier and then used in trajectory calculations.[29] Parts of a global PES were calculated by Banichevich *et al.*[23] and by Borowski *et al.*[24] Recently, Xie *et al.*[27] presented an accurate *ab initio* PES, however, only for near-equilibrium geometries. A very precise PES has been constructed by Tyuterev *et al.*[30,31] by fitting experimental transition energies. Since only states up to about 5800 cm^{-1} above the ground vibrational level were included in the fit, the part of the PES which is most essential to kinetic studies is probably not reliably described by this potential.

In a recent Communication we described the construction of a global PES of ozone in the ground electronic state which has spectroscopic accuracy.[19] In the present paper we give a full account of the electronic structure calculations and the bound state calculations employing this PES. It is organized in the following way: In Sec. II we describe the *ab initio* calculations and the analytical representation of the PES and discuss the essential features. The dynamics calculations are summarized in Sec. III. The results, i.e., the transition energies for all bound states of $^{16}O_3$ are presented and compared to experimental data in Sec. IV; the term energies of several isotopomers are also compared to experimental energies. An analysis of the classical phase space structure in terms of periodic orbits, Sec. V, provides additional clues about the vibrational spectrum of ozone. Finally, a summary concludes this paper in Sec. VI.

II. POTENTIAL ENERGY SURFACE

A. Computational methods

An accurate description of the O–O bonds in ozone needs a large atomic basis set. Earlier studies of the ground and the first excited states of ozone have suggested that one should use at least a triple zeta basis set.[22,24,25] In the present work we go one step further and employ Dunning's standard correlation consistent polarized quadruple zeta (cc-pVQZ) basis set $(12s,6p,3d,2f,1g)/[5s,4p,3d,2f,1g]$.[32] Recent studies of Müller *et al.* on O_2 and O_3 have shown that energies and geometries obtained with this basis set are in good agreement with experimental data.[22,33] Moreover, these results are also in very good agreement with those obtained after extrapolation to a complete basis set; dissociation energies differ by less than 0.1 eV and the bond lengths differ by less than $0.005a_0$.[33]

As we are interested in ozone formation and dissociation, a consistent description of the ground-state PES requires a multiconfigurational ansatz. With the cc-pVQZ basis set a full valence complete active space SCF (CASSCF)[34,35] calculation is possible. However, a realistic description of the bond breaking needs to include also dynamic correlation effects, which can be accounted for by, e.g., multireference configuration interaction (MRCI) calculations.[36,37] But, MRCI calculations using full valence CASSCF wave functions are not affordable for the whole PES—when thousands of nuclear geometries are considered. So, we restrict the active space to molecular orbitals mainly built on the $2p$ orbitals (12 electrons in nine orbitals) whereas the other $1s$ and $2s$ orbitals (6 MOs) are kept doubly occupied but optimized during the CASSCF procedure [CASSCF(12,9)]. The dynamic correlation is taken into account by the internally contracted MRCI method of Werner and Knowles,[36,37] and the Davidson correction[38] is used to approximately estimate the effects of higher excitations [icMRCI+Q]. In a recent study Müller *et al.*[33] have shown that the icMRCI+Q method gives results for the dissociation energy of O_2 (and other diatomic molecules) in good agreement with results obtained with the multireference average quadratic coupled cluster (MR–AQCC) method,[39,40] which—unlike the MRCI method—is size extensive. Along the same line, additional MR–AQCC calculations along the minimum energy path of ozone demonstrate that the icMRCI+Q calculations are reliable; these calculations are part of a more elaborate investigation of the long-range region of the ozone PES and its influence on cross sections and rate constants and will be published elsewhere.[41] In all calculations, the reference function is the same as the CASSCF active space and the frozen core approximation is used, i.e., only the $1s$ orbitals are frozen and not correlated.

In summary, the level of the present calculations can be described as icMRCI+Q/cc-pVQZ using a CASSCF(12,9) reference space. All electronic structure calculations are carried out with the MOLPRO suite of *ab initio* programs.[42]

B. Construction of potential energy surface

It is well known[43–46] that the ozone molecule has two types of minima: one of C_{2v} symmetry (referred to as open minimum) with an apex angle of 116.8° and one of D_{3h} symmetry (ring minimum) in which the oxygen atoms form an equilateral triangle. By virtue of symmetry, there are three equivalent open minima (see below) and therefore the global PES of ozone has four equilibrium structures. The ring minimum lies significantly above the open minima. A description

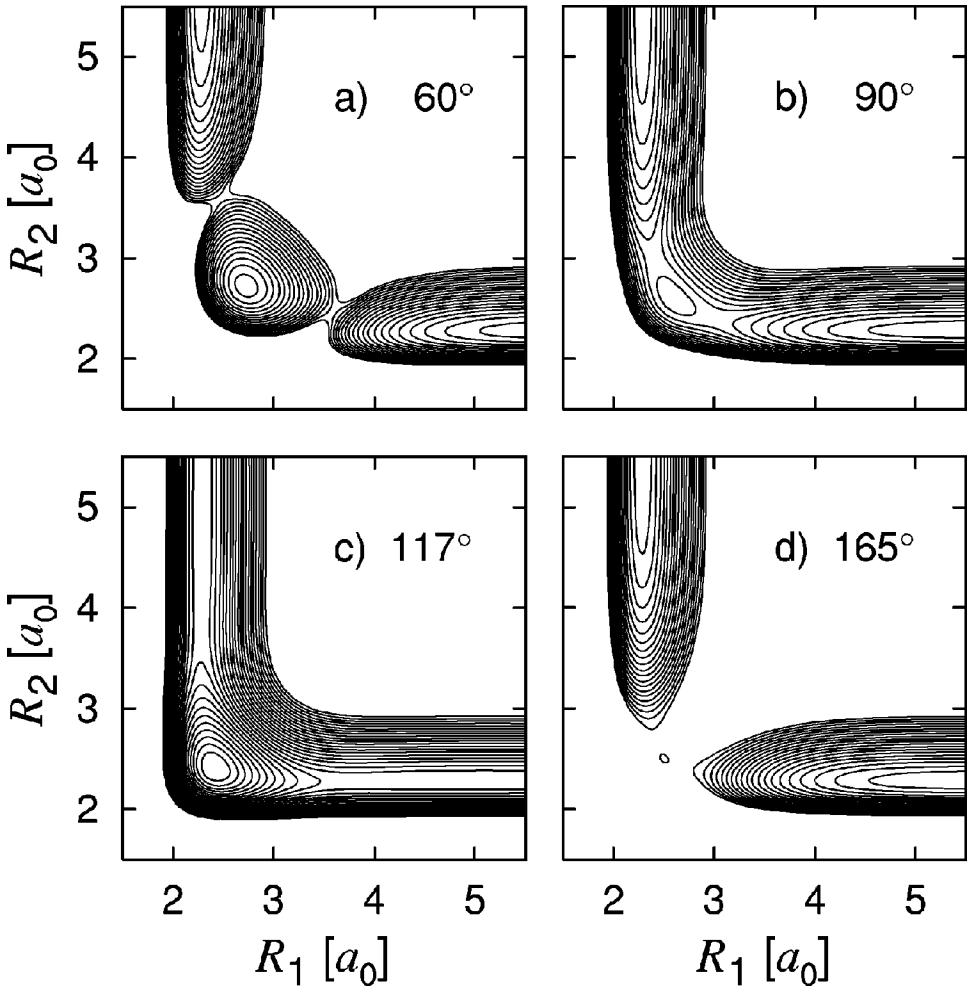

FIG. 1. Contour plots of the ground-state PES of ozone as function of the two O–$\overline{\text{O}}$ bond distances, R_1 and R_2, for fixed bond angle α as indicated; $\overline{\text{O}}$ is the center atom. The highest contour is for $E=3$ eV and the spacing is $\Delta E=0.1$ eV. Energy normalization is so that $E=0$ corresponds to the global minimum.

of the entire PES, in which all three oxygen atoms are treated equivalently, should use coordinates which reflect the full symmetry, for example, perimetric coordinates.[47] However, these coordinates are not convenient for constructing global PES's, including the asymptotic channels. Moreover, the internal motion of the molecule is difficult to rationalize in these coordinates. Therefore, they have not been employed in this study. The three open minima are separated by high barriers (see below) and therefore can be viewed to be independent of each other, at least for the bound states. Ozone in its ground electronic state can be treated as a molecule having C_{2v} symmetry. Therefore, the PES is constructed in terms of the two bond coordinates R_1 and R_2, that is, the two O–$\overline{\text{O}}$ distances, and the O–$\overline{\text{O}}$–O bond angle α, where $\overline{\text{O}}$ is the center atom. These coordinates allow one to take into account the C_{2v} symmetry of the open minima, whereas they are not appropriate to take advantage of the D_{3h} symmetry.

In order to avoid errors due to fitting the calculated energies to an analytical expression, we decided to use interpolation with a three-dimensional cubic spline. However, this requires energies to be calculated on a regular (not necessarily equidistant) and dense grid. In our calculations, one of the distances is varied from $1.9a_0$ to $3.2a_0$ with $\Delta R=0.1a_0$ between $1.9a_0$ and $2.6a_0$ and $\Delta R=0.2a_0$ otherwise. The other distance is varied from $1.9a_0$ to $10.0a_0$ with $\Delta R=0.1a_0$ for 1.9–2.8, $\Delta R=0.2a_0$ for 3.0–4.0, $\Delta R=0.25a_0$ for 4.25–5.0, $\Delta R=0.5a_0$ for 5.5–8.0, and $\Delta R=1.0a_0$ for 9–10, respectively. Only points with $R_2 \leqslant R_1$ are calculated. The angular grid ranges from 60° to 175° with $\Delta\alpha=5°$ for 60–90, $\Delta\alpha=5°$ for 100–110, $\Delta\alpha=5°$ for 125–135, and $\Delta\alpha=10°$ for 145–175; in addition, calculations have been done for 112.5°, 117°, and 121° (20 angles altogether). The small step length around 117° has been chosen in order to increase the accuracy of the PES in the open minimum. The small step length between 60° and 90° is necessary, because here the potential energy changes drastically because of an avoided crossing with another state (see below). In the present study, the ground state is always defined as the lowest *adiabatic* state with $^1A'$ symmetry. Altogether ca. 5000 points on the 3D grid have been determined. By construction, the analytical PES exactly reproduces the calculated energies. A similar strategy has been adopted by Wu *et al.*[48] to construct an accurate PES for the reaction H_2+OH. Potential energies for $\alpha<60°$ can be generated from the spline

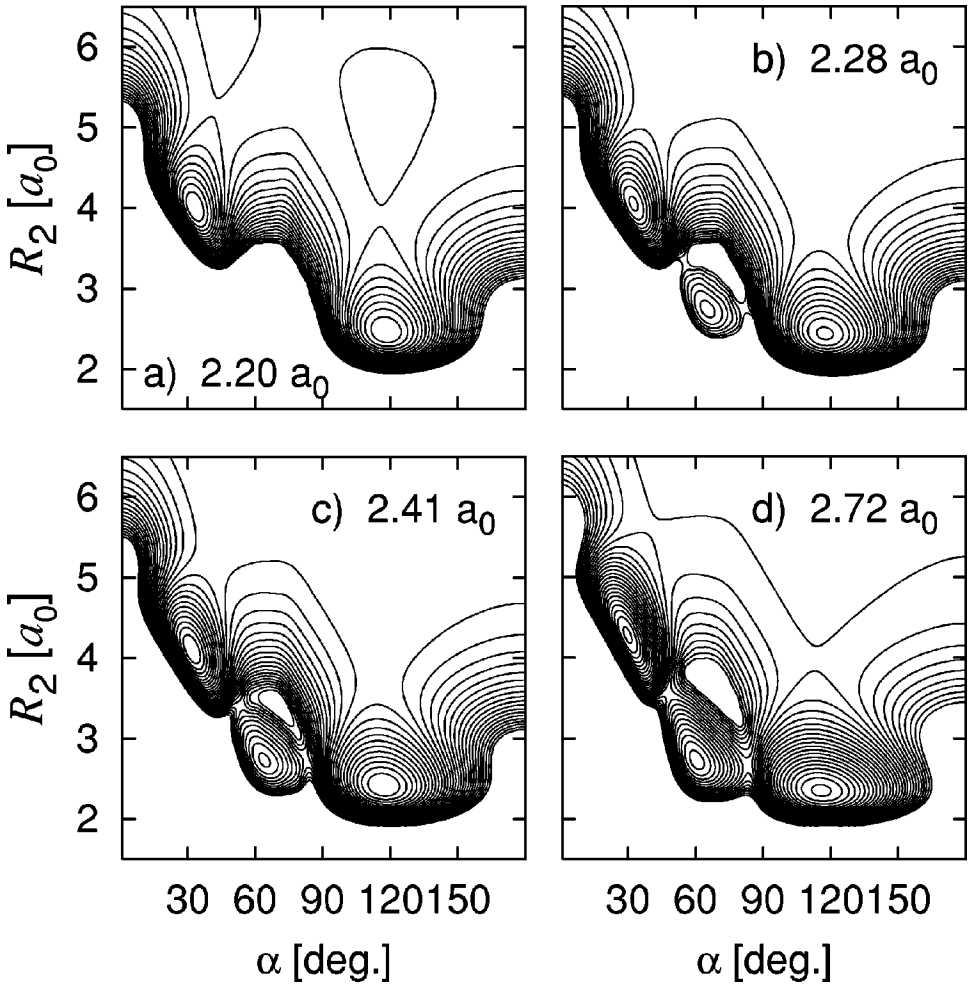

FIG. 2. Contour plots of the ground-state PES of ozone as function of one of the O–$\overline{\text{O}}$ bond distances, R_2, and the O–$\overline{\text{O}}$ bond angle, α; $\overline{\text{O}}$ is the center atom. The other O–$\overline{\text{O}}$ bond distance is fixed as indicated. The highest contour is for $E=3$ eV and the spacing is $\Delta E=0.1$ eV. Energy normalization is so that $E=0$ corresponds to the global minimum.

expression for $\alpha>60°$. We believe that the very good agreement of the calculated vibrational energies with the experimental ones is based—in addition to the high level of the electronic structure theory—on the dense grid and the spline interpolation. All calculated energies are available via EPAPS.[49] The FORTRAN program generating the PES can be obtained from one of the authors (R.Sch.).

Two-dimensional contour plots of the PES are depicted in Figs. 1 and 2. The minimum in Fig. 1(a) is the ring minimum whereas the minimum in Fig. 1(c) is one of the three open minima. The minima near 35° and 117° in each of the panels in Fig. 2 are two of the three open minima. The minimum around 60°, clearly seen in Figs. 2(b)–2(d), is the ring minimum. The small wiggles in the regions of the ring minimum and the barrier between the ring minimum and the open minima are due to the large variation of the potential energy near the conical intersection. However, the wiggles occur at energies high above the dissociation limit and therefore are not expected to influence the bound state calculations or scattering calculations at low energies. Contour plots in terms of perimetriccoordinates, which preserve D_{3h} symmetry,[47,50] are available from EPAPS.[49] In what follows energy normalization is such that $E=0$ corresponds to the global minima, if not stated otherwise.

C. Main features of the PES

In the following we discuss the structures of the two types of minima in more detail. The results for the geometries and the energies of important points on the ground-state PES, as obtained from the spline representation, are reported in Table I, together with other recent theoretical results and experimental data.

1. Open minimum

In the open minimum the ground electronic state has $^1A_1$ symmetry and its electronic configuration, in C_{2v} symmetry, may be described as

$$\text{(I)}\quad (1a_1)^2(1b_1)^2(2a_1)^2(3a_1)^2(4a_1)^2(2b_1)^2 \times(5a_1)^2(3b_1)^2(6a_1)^2(1b_2)^2(4b_1)^2(1a_2)^2(2b_2)^0$$

with the convention that the y axis is perpendicular to the molecular plane. As already noted,[22] this configuration only accounts for 81% of the CASSCF wave function, which un-

TABLE I. Characteristic features of the $O_3(\tilde{X})$ potential energy surface.

	R_1	R_2	α	Energy	D_0
Open minimum	2.4094[a]	2.4094	116.79	1.027[b]	0.944
Expt.	2.4052[c]	2.4052	116.75	1.132[b,d]	1.052[e]
Theor. (Ref. 27)	2.4081	2.4081	116.86	1.049	
Theor. (Ref. 22)	2.4026	2.4026	116.9	1.076	
Ring minimum	2.7249	2.7249	60.00	1.34[f]	
Theor. (Ref. 22)	2.717	2.717	60.00	1.27[f]	
Theor. (Ref. 53)	2.715	2.715	60.00	1.26[f]	
TS open/ring	2.68	2.68	83.1	2.37[f]	
Diss. barrier	3.82	2.28	115.3	0.006[g]	
vdW minimum	4.81	2.28	116.4	0.020[h]	

[a]Distances in a_0, angles in deg., and energies in eV.
[b]Dissociation energy D_e.
[c]Equilibrium bond distances and bond angle from Refs. 30 and 31.
[d]Cited in Ref. 27.
[e]Reference 52.
[f]Energy above open minimum.
[g]Barrier height, with respect to the $O+O_2$ asymptote.
[h]Depth of van der Waals minimum.

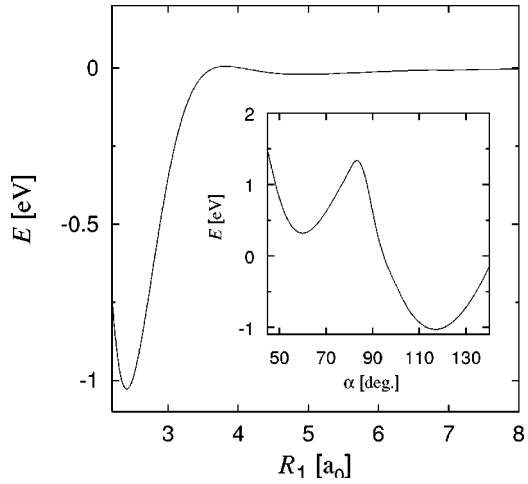

FIG. 3. Potential energy along the minimum energy path as one of the end atoms is removed. The inset shows the minimum energy path for isomerization from the open to the ring minimum. Energy normalization in both figures is so that $E=0$ corresponds to the $O+O_2$ asymptote.

derlines the need for a multiconfiguration description. The second main configuration corresponds to a $(1a_2)^2 \rightarrow (1b_2)^2$ excitation and accounts for another 10% of the wave function,

$$\text{(II)} \quad \ldots(5a_1)^2(3b_1)^2(6a_1)^2(1b_2)^2(4b_1)^2(1a_2)^0(2b_2)^2.$$

In C_s symmetry these two configurations correlate with

$$\text{(Ia)} \quad (1a')^2(2a')^2(3a')^2(4a')^2(5a')^2(6a')^2(7a')^2 \times (8a')^2(9a')^2(1a'')^2(10a')^2(2a'')^2(3a'')^0$$

and

$$\text{(IIa)} \quad \ldots(7a')^2(8a')^2(9a')^2(1a'')^2(10a')^2 \times (2a'')^0(3a'')^2,$$

respectively.

At the icMRCI+Q/cc-pVQZ level, the equilibrium bond length is $2.4094a_0$ and the apex angle is 116.79°, in very good agreement with the values obtained from fitting the experimental rovibrational transition energies,[30,31] $2.4052a_0$ and 116.75°, as well as the results of other recent theoretical studies (Table I). The dissociation energy is calculated to be $D_e=1.027$ eV in good agreement with the previous results of Xie *et al.* (1.049 eV) and Müller *et al.* (1.076 eV). However, our value is about 0.1 eV lower than the experimental value of 1.132 ± 0.017 eV.[51] This discrepancy may have two origins, the basis set or the method of calculation. Increasing the basis from cc-pVQZ to cc-pV5Z[22,41] increases D_e to 1.098 eV. Extrapolation to a complete basis set leads to a dissociation energy of 1.116 eV,[41] in excellent agreement with the experimental value. Considering, on the other hand, the level of calculation, two effects have to be taken into account, which may change the dissociation energy in opposite directions. First, excluding the $2s$ orbitals from the active space worsens the description of the O–O sigma bonds. Consequently, as there are two sigma bonds in O_3 and only one in O_2+O, using a restricted active space at the CASSCF level leads to an underestimation of the dissociation energy. This effect has been estimated by Müller *et al.* at the MRCI/cc-pVQZ level to be approximately 0.1 eV. On the other hand, the internally contracted scheme together with the Davidson correction tends to overestimate the dissociation energy. Comparing the dissociation energies obtained from icMRCI+Q and from MR–AQCC methods, in both calculations using the cc-pVQZ basis, shows that this effect is approximately 0.05 eV. Thus, the best calculation, within the framework of the present study, is expected to give a dissociation energy about 0.03 eV larger than the experimental value.

Very important for the reaction dynamics is the shape of the PES along the dissociation path. Two distinct paths can be considered for the dissociation starting in the open minimum. The first one is defined by removing the central oxygen atom while retaining C_{2v} symmetry. The second one essentially corresponds to cutting the bond of one of the two identical end atoms with the apex angle remaining around 116°. As the first path preserves C_{2v} symmetry, the use of a Woodward–Hoffman correlation diagram is appropriate. It shows that this path is not energetically favorable; it leads to a very high barrier which is located more than 3.6 eV above the open minimum, that is more than 2 eV above the dissociation limit.

The potential energy along the minimum energy path (MEP) for the removal of an end atom is depicted in Fig. 3. As already noted in earlier investigations,[19,23,25,46] there is a barrier at intermediate $O-O_2$ separations. In our calculations, the barrier is only 0.006 eV above the dissociation limit and it is located at $R_1=3.82a_0$, $R_2=2.28a_0$, and $\alpha=115.3°$. In the previous studies it is significantly higher. This barrier is caused by an avoided crossing between the ground state of ozone ($^1A'$ in C_s symmetry) and one of the states which emerge from the $O_2(^3\Sigma_g^-)+O(^3P)$ asymptote. The main configurations of the open minimum [(Ia) and (IIa)] correlate diabatically with the first excited singlet states of the products, $O_2(^1\Delta_g)+O(^1D)$, which are approximately 3 eV above the corresponding ground states. On the other hand, the combination of $O_2(^3\Sigma_g^-)$ and $O(^3P)$ leads to three singlet states,

two having A' symmetry and one with A'' symmetry. All these states have an open shell (with four unpaired electrons) and do not correlate to the ground state of the open minimum. As a consequence, there is an avoided crossing between the (diabatic) state that corresponds mainly to configurations (Ia) and (IIa) and the lowest $^1A'$ state that correlates with the $O_2(^3\Sigma_g^-)+O(^3P)$ asymptote. Beyond the barrier there is a shallow van der Waals minimum (Table I).

An accurate description of the barrier thus must involve a good description of these two diabatic states, that is, a good description of the O_3 open minimum, of the ground-state products, as well as the first excited singlet states of O_2 and O. A prerequisite is a reliable estimation of the energy of the excited states of the O_2+O system. At the icMRCI+Q/cc-pVQZ level, the first excited state ($^1\Delta_g$) of the oxygen molecule is located 0.997 eV above the ground state energy ($R=2.2860a_0$), in good agreement with the corresponding experimental value of 0.982 eV. The first excited state of the oxygen atom (^3P) is located 2.029 eV above the ground state, which also agrees well with the experimental value, 1.967 eV. The calculated excitation energy $O_2(^3\Sigma_g^-)+O(^3P)\rightarrow O_2(^1\Delta_g)+O(^1D)$ is thus 3.026 eV, slightly larger than the experimental value of 2.949 eV. In view of these estimates we can expect that the icMRCI+Q/CASSCF(12,9) method is well adapted to describe the dissociation for the open minimum.

The barrier depends sensitively on the atomic basis size. It is about 0.13 eV for the cc-pVDZ basis and 0.055 eV for the cc-pVTZ basis. Using the cc-pV5Z basis pushes the barrier below the asymptote. Nevertheless, it is still meaningful to speak of a barrier, because the van der Waals minimum is below the saddle point. This general picture is not qualitatively changed when an extrapolation to the complete basis set limit is made. In a future publication we will investigate the influence of this barrier and the general shape of the PES in the region of the transition state on the reaction dynamics.[41] The transition state (TS) is very tight—compared to the model PES assumed by Gao and Marcus.[17] The lowest frequency at the barrier is 267 cm^{-1} on our PES.

2. Ring minimum

The main two configurations (in C_{2v} symmetry) of the ring minimum are

$$\text{(III)} \quad \ldots(5a_1)^2(3b_1)^2(6a_1)^2(1b_2)^2(1a_2)^2(2b_2)^2(4b_1)^0,$$

$$\text{(IV)} \quad \ldots(5a_1)^2(3b_1)^2(6a_1)^0(1b_2)^2(1a_2)^2(2b_2)^2(4b_1)^2;$$

they account for 87% and 2% of the CASSCF wave function, respectively. The energy is 1.34 eV higher than the energy of the open minimum and the O–O bond length is significantly larger, $R=2.7249a_0$ compared to $R=2.4094a_0$. These results are compared in Table I to those of earlier theoretical studies.[22,53] Experimental data do not exist. Our values are in good agreement with the data of Müller *et al.* calculated at the MRCI/cc-pV5Z level using a full valence CASSCF reference space as well as the calculations of Lee who used the CCSD(T) level of theory and a large atomic basis. In our calculations, the energy of the ring minimum (with respect to the energy of the open minima) is approximately 0.07–0.08 eV higher than in the calculations of Müller *et al.*[22] and Lee,[53] respectively. The ring minimum has three sigma bonds, that is one more than the open minimum. Consequently, the use of a restricted active space should lead to an overestimation of its relative energy.[22]

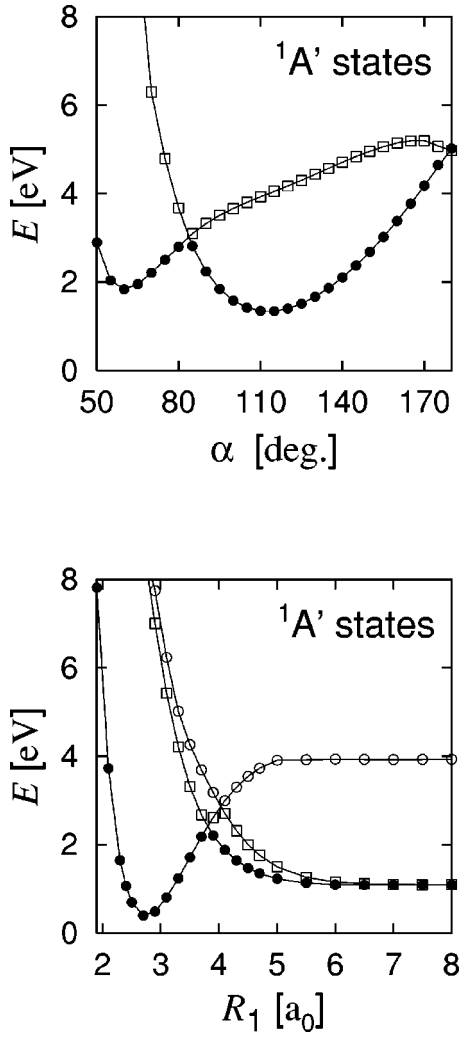

FIG. 4. Upper panel: Cut along the bond angle α for $R_1=R_2=2.725a_0$. Lower panel: Cut along R_1 for $R_2=2.725a_0$ and $\alpha=60°$. The symbols are the calculated points. The filled circles represent the lowest adiabatic PES. For more details see the text.

There have been controversies about the position of the ring minimum with respect to the dissociation limit. Today, it is beyond question that it lies *above* the dissociation energy of the ground state.[22,25,53] As for the open minimum, the main configurations (III) and (IV) correlate diabatically with the first excited singlet state of the O_2+O system. This is illustrated in Fig. 4 where we show two cuts through the equilibrium of the ring minimum. They have been obtained at the icMRCI+Q level with a cc-pVTZ basis set, using a restricted CAS(12,9) wave function. The lowest two, respectively, three states of A' symmetry are calculated simultaneously, which explains the use of the smaller basis in preparing these cuts. The symbols represent the adiabatic states whereas the lines through the points indicate the diabatic potential curves; the latter have not been calculated in a diabatization scheme, but are drawn by hand. The filled circles

represent the lowest adiabatic state. The icMRCI+Q/cc-pVTZ energy of the ground state of O_2+O with O_2 at its equilibrium geometry ($R_1=2.2833a_0$ at the icMRCI+Q/cc-pVTZ level) is used as the reference energy.

In the lower panel of Fig. 4 the (asymptotically) two lower states dissociate to ground-state products $O_2(^3\Sigma_g^-)+O(^3P)$. Because R_2 is kept fixed at $2.725a_0$, the energy of O_2 is 1.1 eV higher than for the equilibrium geometry. The third A' state dissociates to the first excited singlet state of O_2+O, located 2.83 eV above the ground state. As a consequence of the avoided crossing there is a high barrier along the dissociation path. For the R_1 cut shown in the figure, this barrier is located at $R_1\approx 3.8a_0$ and is 2.4 eV higher than the dissociation limit. As seen from Fig. 2, this high barrier exists also for other R_1 cuts through the PES: The ring minimum is encircled by a high ridge with saddle points connecting to the three open minima. No direct path leads from the ring minimum to the product channels; the energetically most favorable path for removal of an oxygen atom goes through one of the open minima.[25] A cut through the ring minimum along α is shown in the upper panel of Fig. 4. Thebarrier caused by the avoiding crossing is also clearly seen in this representation. For this particular cut the barrier occurs at $\alpha\approx 84°$ and its height is about 3.0 eV. In accordance with the results of Ruedenberg and co-workers[25,54] we have found the transition state for isomerization from the ring to the open minimum to occur in C_{2v} symmetry ($R_1=R_2=2.68a_0$ and $\alpha=83.1°$). In our calculations, it occurs 1.02 eV above the ring minimum (inset of Fig. 3). Because the conical intersection happens high above the dissociation limit, no attempt for a proper diabatization has been made. The nonadiabatic coupling between the lowest two $^1A'$ states in the region between the open minima and the ring minimum recently has been studied by Sukumar and Peyerimhoff.[55]

In conclusion, the ring minimum cannot be accessed at low and intermediate collision energies and therefore it is not expected to play a significant role in the formation and dissociation of ozone. Incidentally we note, that Plass *et al.*[56] have claimed to have identified cyclic ozone (ring minimum) in magnesium oxide (111) surface recombination. The vibrational spectroscopy of cyclic ozone will be discussed elsewhere.[57]

III. DYNAMICS CALCULATIONS

The dynamics calculations are performed using the filter diagonalization method.[58–60] In the first step, optimally adapted basis functions Ψ_i for a given energy interval $[E_{\min},E_{\max}]$ are constructed by applying the Green's function $\hat{G}^+(E_i)=(E_i-\hat{H}+iW)^{-1}$ as a filtering operator onto an initial wave packet χ_0,

$$\Psi_i=\mathrm{Im}\{\hat{G}^+(E_i)\,\chi_0\}. \tag{1}$$

Here, iW represents a complex absorbing potential,[61–63] which enters the filtering procedure in form of a damping operator $\exp(-\hat{\gamma})$. Strictly speaking, an absorbing potential is not needed for the calculation of bound states, at least not for low-lying ones, and therefore details are not presented here. The filtering is efficiently performed by employing the Chebychev polynomial expansion of the Green's function,[59,60,64,65] which is global in energy. In the second step the spectral information in the given energy window is extracted by diagonalizing the Hamiltonian in the small (250–300) set of basis functions Ψ_i.

Because the barrier to isomerization (open → ring → open) is about 1.3 eV with respect to the dissociation asymptote, for the calculation of bound states it suffices to consider only one of the three open minima. Every coordinate system which takes proper account of the remaining C_{2v} symmetry and in which the kinetic energy operator has a simple diagonal form, like Radau or Jacobi coordinates, is appropriate. In the present calculations, we employ Jacobi coordinates defined as follows: R is the distance from the central oxygen atom to the center-of-mass of the two end atoms, r is the distance of the two end atoms, and γ is the angle between these two vectors. In this way the symmetry of the two dissociation channels can be easily incorporated: The wave functions are either symmetric or antisymmetric with respect to $\gamma=90°$. When one of the end atoms is pulled away towards dissociation, both r and R are elongated. Jacobi coordinates defined so that R connects one end atom and the center-of-mass of the other two atoms, as they are usually used in collisions, do not reflect the C_{2v} symmetry.

After some test calculations we have chosen the coordinate ranges $0.1a_0\leqslant R\leqslant 9.0a_0$ with 120 potential-optimized points,[66] $3.0a_0\leqslant r\leqslant 10.0a_0$ with 100 such points, and $0\leqslant\gamma\leqslant 180°$ with 80 Gauss–Legendre quadrature points.[67] All points of the three-dimensional grid with a potential energy larger than 3.0 eV (with respect to the global minimum) are discarded, which reduces the number of grid points to about 220 000. With these parameters, the spectral range of the Hamiltonian, ΔH, is about 25 eV. For this value of ΔH and the density of states of 0.07 states per cm^{-1} at the dissociation threshold a rule of thumb[59] predicts 50 000 Chebychev iterations to be sufficient for creating a good basis $\{\Psi_i\}$, and indeed this was found to be correct. The initial wave packet χ_0 is random to insure non-vanishing overlap with all states; however, it is located only in the interior part of one of the open minima in order to maximize overlap with the bound states only. In the case of the ABA isotopomers, the symmetry of the wave functions with respect to $\gamma=90°$ is accounted for in the following way (see also Ref. 68). First, an asymmetric wave packet is propagated yielding basis functions Ψ_i, which also have no particular symmetry. In the second step, these basis functions are symmetrized or antisymmetrized. Finally, the Hamiltonian is diagonalized in the basis of either the symmetric or the antisymmetric functions.

In addition to these filter-diagonalization calculations we performed calculations with slightly different parameters and employed the harmonic inversion algorithm[69,70] for obtaining the bound state energies. The energy levels agreed within a small fraction of a cm^{-1}.

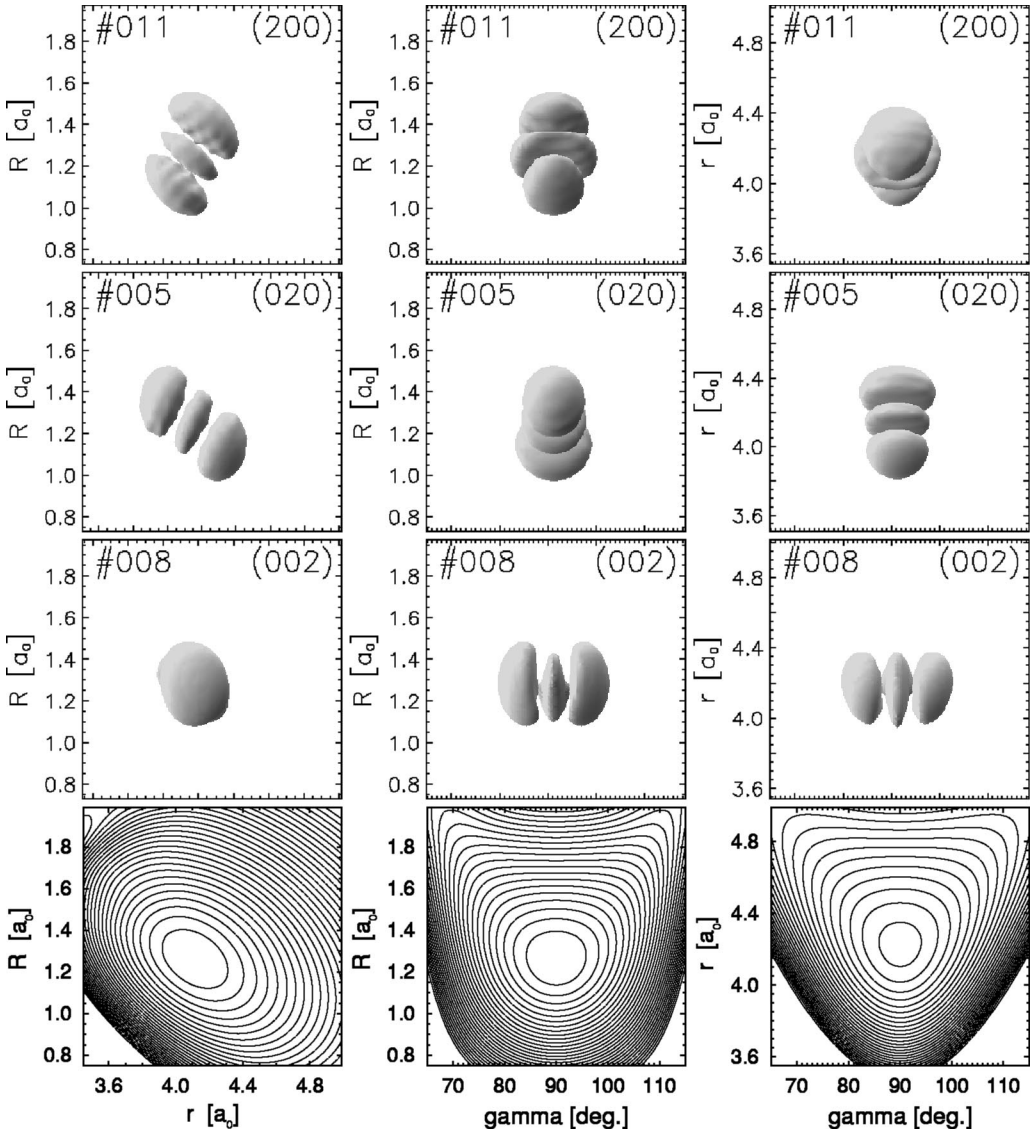

FIG. 5. Wave functions for states (2,0,0), (0,2,0), and (0,0,2) in three different coordinate representations. Shown is one particular contour $\epsilon(R,r,\gamma)=|\Psi(R,r,\gamma|^2$ with the value of ϵ being the same in one figure. The plots are viewed along one coordinate axis, in the direction perpendicular to the plane of the other two coordinates. Shading emphasizes the 3D character of the wave functions. The number in the upper left corner of each panel is the number according to Table II and the number in the upper right corner is the assignment. The lower panels show the corresponding representations of the PES.

IV. RESULTS

A. Wave functions and assignments

All states up to 99% of the (calculated) dissociation energy—plus a few extra states of the overtone progressions located in the continuum—have been calculated and analyzed. Each wave function has been visually inspected by a three-dimensional plotting routine in order to assign quantum numbers. In what follows, v_1, v_2, and v_3 are the symmetric stretch, the bend, and the antisymmetric stretch quantum numbers, respectively. In order to illustrate the shapes of the wave functions in terms of the Jacobi coordinates R, r, and γ used in the present study, the wave functions for the overtone states (2,0,0), (0,2,0), and (0,0,2) are shown in Fig. 5. Because the wave functions are not aligned along either one of the three planes, it is very helpful to consider all three planes: (R,r), (R,γ), and (r,γ). Symmetric stretch excitation is best seen in the (R,r) plane: R and r increase/decrease simultaneously. Bending excitation is clearly seen in the (R,r) or the (r,γ) plane; when the ozone molecule bends, r increases whereas R decreases and γ remains unchanged. Finally, antisymmetric stretch motion is most obviously recognized in the (r,γ) representation; r remains unchanged while γ varies considerably. The wave functions for the ABA isotopomers are either symmetric (v_3 even) or antisymmetric (v_3 odd) with respect to $\gamma=90°$. As a consequence, they have either a maximum or a minimum at 90° or a node in the latter case. Of course, ABB or ABC isotopomers do not have this symmetry.

Using other coordinate representations would yield different wave function pictures. However, the assignment does not depend on the coordinates used. If a wave function has a complicated nodal structure which prohibits a clear-cut assignment, it is unlikely that other coordinates give simpler pictures. The complicated nodal structure is the result of

mixing between two or more almost degenerate states and this mixing does not depend on the coordinate system employed.

The assignment in terms of v_1, v_2, and v_3 is a normal-mode assignment. Alternatively, one could employ a local-mode assignment, which for ABA molecules may have certain advantages.[71,72] A local-mode description of the vibrational states of ozone up to the dissociation threshold, has been provided by Pérez-Bernal *et al.*[73] using an algebraic Hamiltonian. In the present study we nevertheless use the standard normal-mode analysis for several reasons: (i) All experimental assignments are based on a normal-mode description; (ii) the normal-mode assignment yields a reasonable description up to high energies; and (iii) local-mode character is observed only for a relatively small number of states at higher excitation energies (see below).

The complete list of energies and assignments, provided they are possible, are listed in Table II. Up to an excitation energy of about 6800 cm^{-1} all states can be unambiguously assigned, with only few exceptions. This is particularly true for those states for which experimental data are available; they are mainly limited to transition energies smaller than 6500 cm^{-1} or so (see Table II). As energy increases, gradually more and more states possess wave functions, which do not allow a clear-cut assignment. In some of these cases, however, the energetic positions and/or the symmetry of the wave function allow one to find, nevertheless, meaningful quantum numbers (in terms of progressions rather than nodal structures). The wave functions of all states are published electronically.[49]

The pure progressions $(v_1,0,0)$, $(0,v_2,0)$, and $(0,0,v_3)$, the wave functions of which are exhibited in Fig. 6, can be followed without difficulties up to high overtones. This is particularly true for the symmetric stretch and the bend states: They can be clearly assigned even high in the continuum. The antisymmetric stretch states experience some strong coupling with nearby states at intermediate energies with the result that the wave functions for $v_3=5-8$ are heavily mixed with other states of the same symmetry. Higher states of this progression are unbound; because of the excitation in the dissociation mode, these resonance states are rather broad and therefore higher members could not be unambiguously identified. State (0,0,5) is mixed with (3,1,1), both being antisymmetric, and (0,0,7) is coupled with state (4,2,1). State (0,0,6) is possibly mixed with (3,1,2); for (0,0,8) we could not unambiguously identify possible perturbing states. The mixing between (3,1,1) and (0,0,5) has also been discussed experimentally.[74,75] A figure showing the corresponding wave functions can be obtained from EPAPS.[49] Generally speaking, states with many quanta in one mode and few quanta in the two other modes, like (1,8,1), can be clearly assigned even at high energies. On the contrary, states with several quanta in all three modes are difficult to assign already at intermediate energies. In order to demonstrate the complexity of the ozone wave functions we show in Fig. 7 five examples in all three different representations. State No. 170 has no obvious assignment. The assignment of the highly excited states of ozone still raises interesting questions, which are worth to be addressed in future studies using, e.g., spectroscopic Hamiltonians.[76]

B. Polyad structure and local-mode states

The excitation energies of the fundamentals of the stretching modes, 1043.9 cm^{-1} and 1101.9 cm^{-1}, differ by only 58 cm^{-1}. As a consequence, the spectrum is organized in terms of polyads $[v_2,P]$, with $P=v_1+v_3$ being the polyad quantum number. For each bending quantum number v_2, there exist $P+1$ states in a polyad. In the following we will discuss only the polyads for $v_2=0$.

The antisymmetric stretch states $(0,0,v_3)$ are at the bottom of a polyad whereas the symmetric stretch states $(v_1,0,0)$ mark the top of a polyad. The energy range spanned by the polyads strongly increases with P; it is 58 cm^{-1} for $P=1$ and ca. 1000 cm^{-1} for $P=7$. The reason for this substantial variation is the difference in the anharmonicities in the symmetric and antisymmetric stretching modes. The energy differences between adjacent states in the three overtone progressions are depicted in Fig. 8. While the frequency of the symmetric stretch progression decreases only slightly with energy, respectively P, the antisymmetric stretch frequency decreases rapidly with E. The large anharmonicity of the antisymmetric stretching mode reflects the gradual change of the character of the $(0,0,v_3)$ states: With increasing energy, the $(0,0,v_3)$ wave functions gradually acquire more and more local-mode character, i.e., they stretch further and further along the two identical $O_3 \rightarrow O_2+O$ dissociation channels. The local-mode type character of the high overtones of the $(0,0,v_3)$ states becomes evident in Fig. 9 for the (0,0,8) wave function in the (γ,R) representation; the two dissociation channels are seen for large values of R and small/large values of γ. It is not difficult to imagine the (0,0,8) wave function to be the (symmetrized) sum of two wave functions—each being aligned along either one of the exit channels. This will become even clearer in Sec. V where classical periodic orbits and their relationship to the quantum mechanical wave functions will be discussed. At lower energies the alignment of the antisymmetric stretch wave functions along the $O-\overline{O}$ bonds is not so pronounced as illustrated by the (0,0,4) wave function also depicted in Fig. 9. The antisymmetric states exhibit a gradual change from normal- to local-mode character as is well known for ABA molecules.[71,72,77–79]

The $(0,0,v_3)$ states are accompanied by states, which are slightly higher in energy and which in the normal-mode representation are termed $(1,0,v_3-1)$. The energy difference between this pair of states, which have different symmetries, is 58 cm^{-1} for polyad $P=1$ and decreases to about zero for $P=8$. Due to mixing with other states of the same symmetry, the decrease is not monotonic, though. The counterparts to (0,0,4) and (0,0,8), that is, (1,0,3) and (1,0,7), respectively, are also displayed in Fig. 9. For state (1,0,3) the normal-mode assignment is still meaningful. However, for (1,0,7) it is difficult to see the relationship between the quantum numbers and the nodal structure. The local-mode assignments for these pairs of states at the bottom of each polyad are

TABLE II. Vibrational energies (in cm^{-1}) and assignments for $^{16}O_3$.

No.	(v_1,v_2,v_3)[a]	E	No.	(v_1,v_2,v_3)	E	No.	(v_1,v_2,v_3)	E
1	(0,0,0)	0.0	63	(0,6,1)	5093.5	125	(0,7,2)	6648.5
2[b]	(0,1,0)	698.5	64	(2,3,1)	5154.3	126	((2,4,2))	6654.8
3	(0,0,1)	1043.9	65	(3,0,2)	5170.4	127	(3,1,3)	6680.6
4	(1,0,0)	1101.9	66	(1,6,0)	5202.1	128	(0,3,5)	6700.9
5	(0,2,0)	1394.3	67	(0,2,4)	5261.1	129	(1,7,1)	6705.0
6	(0,1,1)	1726.0	68	(1,2,3)	5285.9	130	(5,2,0)	6743.1
7	(1,1,0)	1792.4	69	(3,3,0)	5303.3	131	(1,3,4)	6748.5
8	(0,0,2)	2060.6	70	(4,0,1)	5305.6	132	(4,1,2)	6812.2
9	(0,3,0)	2088.1	71	(0,5,2)	5358.2	133	(3,4,1)	6818.4
10	(1,0,1)	2111.3	72	(2,2,2)	5414.3	134	(2,7,0)	6849.2
11	(2,0,0)	2199.0	73	(1,5,1)	5430.7	135	(0,10,0)	6860.0
12	(0,2,1)	2404.8	74	(5,0,0)	5435.7	136	((2,0,5))	6870.3
13	(1,2,0)	2481.1	75	((0,1,5))	5512.7	137	((2,3,3))	6882.2
14	(0,1,2)	2726.3	76	(0,8,0)	5516.1	138	(0,6,3)	6884.2
15	(0,4,0)	2780.2	77	(1,1,4)	5534.7	139	((0,2,6))	6898.1
16	(1,1,1)	2783.2	78	((3,2,1))	5555.1	140	((3,0,4))	6921.6
17	(2,1,0)	2881.7	79	(2,5,0)	5574.8	141	(1,6,2)	6938.7
18	(0,0,3)	3048.6	80	(0,4,3)	5625.9	142	((1,2,5))	6975.6
19	(0,3,1)	3081.3	81	(1,4,2)	5670.5	143	((5,1,1))	6976.9
20	(1,0,2)	3084.5	82	(2,1,3)	5694.6	144	(4,4,0)	6985.8
21	(1,3,0)	3168.1	83	(4,2,0)	5695.3	145	(2,6,1)	7017.9
22	(2,0,1)	3186.3	84	(0,7,1)	5755.0	146	((3,3,2))	7060.3
23	(3,0,0)	3286.7	85	(0,0,6)	5758.7	147	(0,9,1)	7060.5
24	(0,2,2)	3388.7	86	(1,0,5)	5776.5	148	(4,0,3)	7077.2
25	(1,2,1)	3452.3	87	(2,4,1)	5793.1	149	(0,5,4)	7085.8
26	(0,5,0)	3470.0	88	(3,1,2)	5809.2	150	((1,1,6))	7099.8
27	(2,2,0)	3562.8	89	(1,7,0)	5867.1	151	((0,1,7))	7107.6
28	(0,1,3)	3698.3	90	(0,3,4)	5882.7	152	(1,5,3)	7134.8
29	(1,1,2)	3737.7	91	(1,3,3)	5910.7	153	(6,1,0)	7143.9
30	(0,4,1)	3755.5	92	(4,1,1)	5943.0	154	(1,9,0)	7172.6
31	(2,1,1)	3847.6	93	(3,4,0)	5961.0	155	((4,3,1))	7177.8
32	(1,4,0)	3851.6	94	(2,0,4)	5993.7	156	*s*	7210.4
33	(3,1,0)	3961.8	95	(0,6,2)	6006.7	157	(5,0,2)	7220.8
34	(0,0,4)	4002.1	96	(2,3,2)	6037.9	158	*s*	7225.2
35	(1,0,3)	4021.4	97	(3,0,3)	6060.5	159	((0,4,5))	7257.6
36	(0,3,2)	4048.2	98	(1,6,1)	6073.6	160	((2,5,2))	7260.7
37	(1,3,1)	4118.0	99	(5,1,0)	6094.2	161	(0,8,2)	7288.6
38	(2,0,2)	4142.1	100	(0,2,5)	6114.4	162	*a*	7297.2
39	(0,6,0)	4156.5	101	(1,2,4)	6145.1	163	((0,0,8))	7320.1
40	(2,3,0)	4240.3	102	(0,9,0)	6188.3	164	((1,0,7))	7320.9
41	(3,0,1)	4248.9	103	(3,3,1)	6192.0	165	(1,8,1)	7321.7
42	(0,2,3)	4344.4	104	(4,0,2)	6202.5	166	*s*	7342.2
43	(4,0,0)	4365.8	105	(2,6,0)	6225.2	167	((5,3,0))	7365.2
44	(1,2,2)	4387.0	106	(0,5,3)	6259.2	168	(6,0,1)	7389.9
45	(0,5,1)	4426.6	107	((2,2,3))[e]	6296.6	169	*a*	7414.7
46	(2,2,1)	4504.6	108	(1,5,2)	6304.5	170	*s*	7422.7
47	(1,5,0)	4530.0	109	((0,1,6))	6331.8	171	(3,5,1)	7433.6
48	(0,1,4)[c]	4629.4	110	(5,0,1)	6352.3	172	*s*	7442.8
49	(3,2,0)[c]	4640.0	111	(4,3,0)	6354.8	173	(1,7,2)	7452.1
50	(1,1,3)	4655.9	112	(1,1,5)[e]	6376.9	174	(2,4,3)	7475.7
51	(0,4,2)	4705.1	113	(0,8,1)	6408.4	175	(0,7,3)	7489.7
52	(1,4,1)	4778.2	114	(2,5,1)	6418.6	176	(0,11,0)	7520.0
53	(2,1,2)	4781.7	115	(3,2,2)	6437.0	177	(3,1,4)	7528.1
54	(0,7,0)	4838.7	116	(0,4,4)	6493.8	178	*s*	7528.8
55	(3,1,1)[d]	4893.9	117	(6,0,0)	6496.0	179	(7,0,0)	7547.1
56	(2,4,0)	4911.8	118	(1,8,0)	6524.4			
57	(0,0,5)[d]	4916.6	119	(1,4,3)	6528.7	180	(0,12,0)	8179.5
58	(1,0,4)	4919.3	120	((1,0,6))	6553.4	181	(8,0,0)	8588.5
59	(0,3,3)	4987.1	121	((0,0,7))[f]	6557.2	182	(0,13,0)	8835.5
60	(1,3,2)	5031.1	122	(4,2,1)[f]	6576.2	183	(0,14,0)	9485.3
61	((4,1,0))	5033.6	123	(3,5,0)	6602.8	184	(9,0,0)	9619.3
62	(2,0,3)	5077.6	124	*s*	6620.9	185	(10,0,0)	10642.4

[a]Questional assignments are denoted by double parentheses; if no assignment is possible, at least the symmetry (*s* for symmetric and *a* for antisymmetric) is given.
[b]States for which experimental energies are available are underlined.
[c]Coupling between (0,1,4) and (3,2,0).
[d]Coupling between (3,1,1) and (0,0,5).
[e]Possible coupling between ((2,2,3)) and (1,1,5).
[f]Coupling between ((0,0,7)) and (4,2,1).

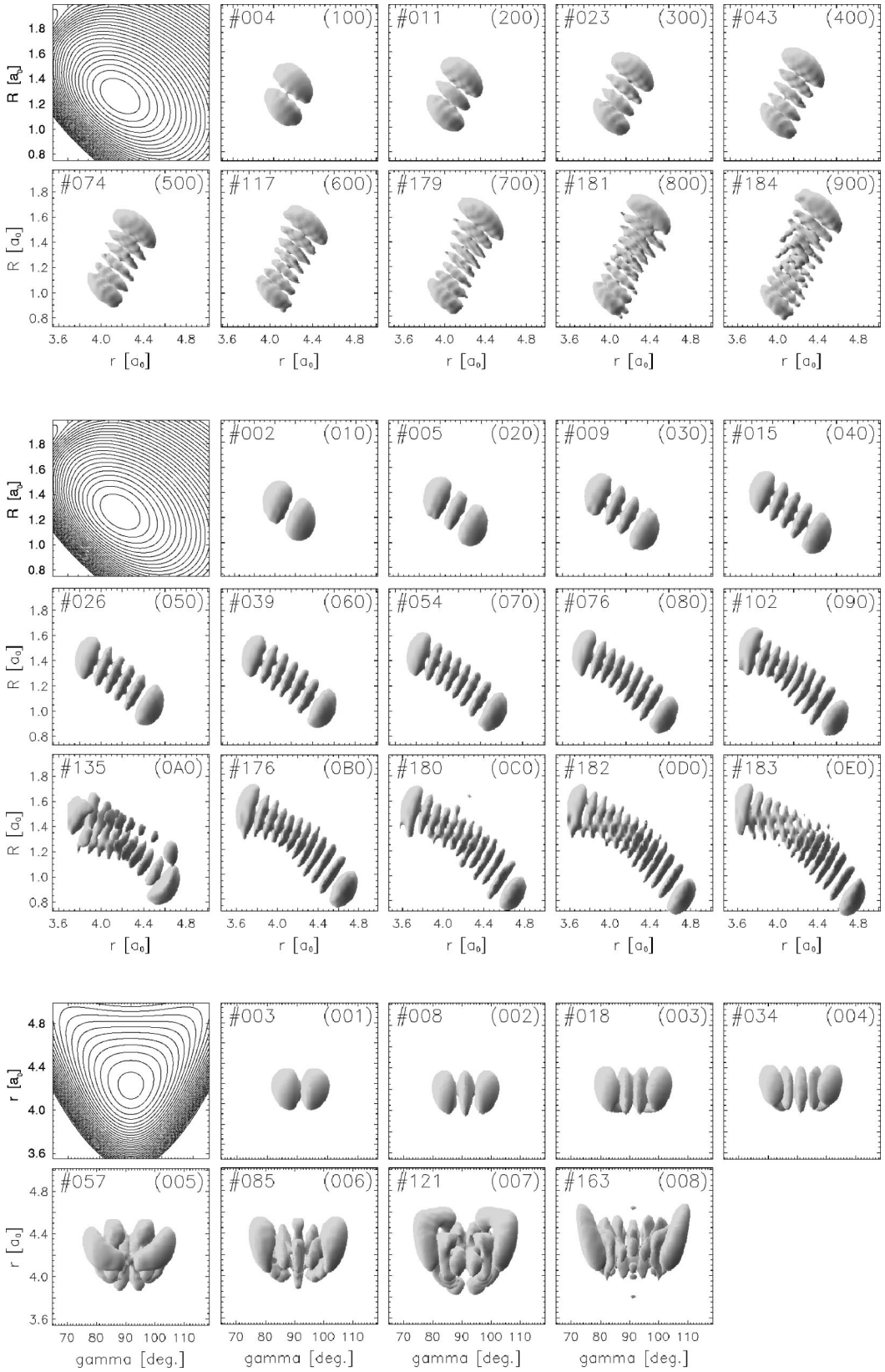

FIG. 6. Wave functions for the overtone states $(v_1,0,0)$ (upper two rows), $(0,v_2,0)$ (middle three rows), and $(0,0,v_3)$ (lower two rows). The first panel of each progression shows the potential. (0A0), (0B0), etc., stand for (0,10,0), (0,11,0), etc. For more details see Fig. 5.

$|v_3,0^{\pm};0\rangle$, where the last number is the bending quantum number. The corresponding wave functions are (ignoring the bending degree of freedom) two-mode symmetric $(+)$ and anti-symmetric $(-)$ oscillator wave functions with v_3 quanta in one O–$\overline{\text{O}}$ bond and zero quanta in the other bond.

The splitting of the states near the bottom of the polyads has been explained by several authors using different models.[80–83] In very vague terms, it depends on the coupling

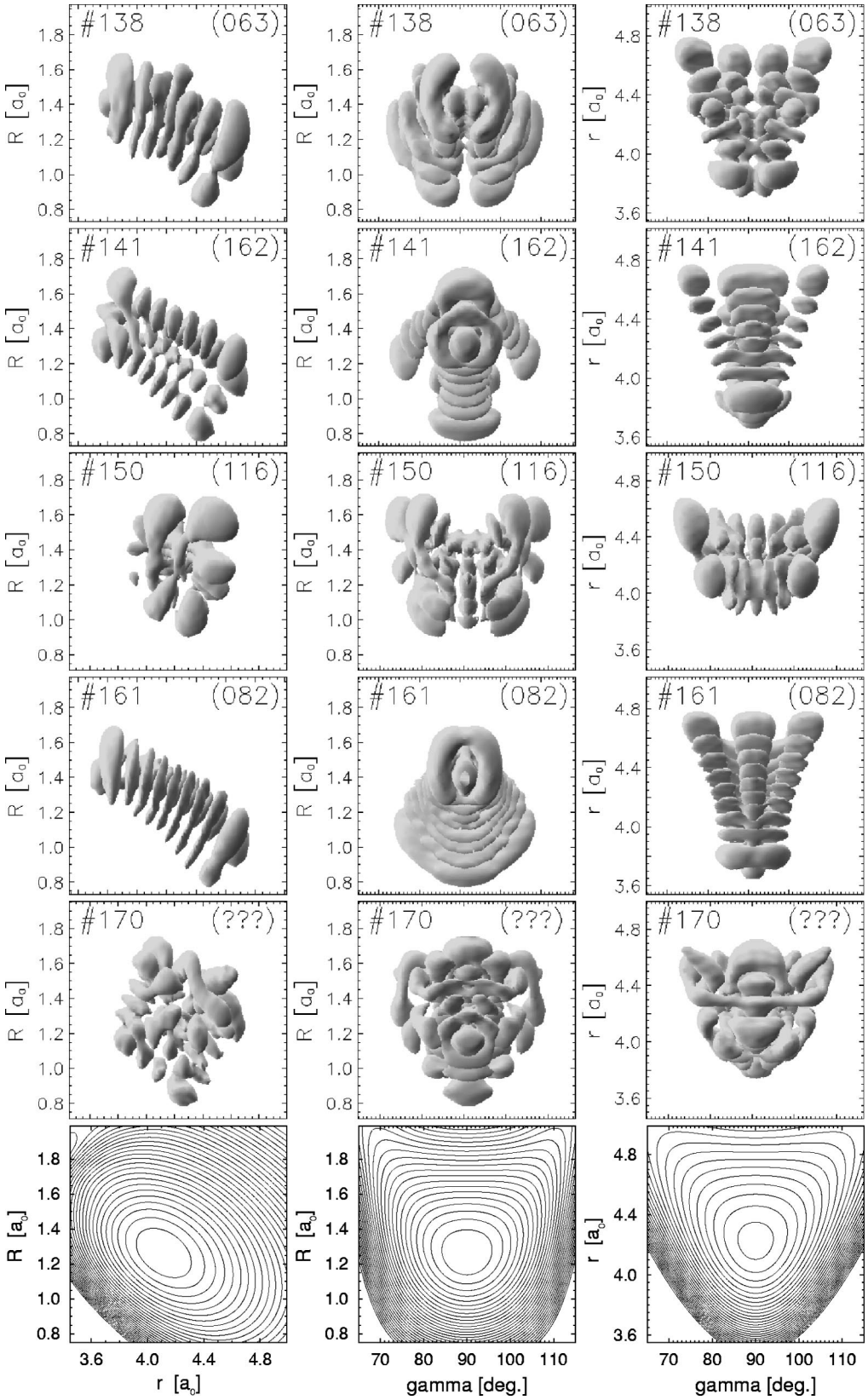

FIG. 7. Wave functions for highly excited states with excitations in at least two modes. For more details see Fig. 5.

between the stretching motions of the two O–$\overline{\text{O}}$ bonds: the weaker the coupling, the smaller the splitting. When the antisymmetric stretching mode is excited, the molecule spends gradually more time in one or the other exit channel. Since the two channels are—asymptotically—separated by a high ridge, it is plausible to assume that the net coupling between the two bonds gradually becomes weaker; thus, the splitting decreases with P. There are, of course, other almost degen-

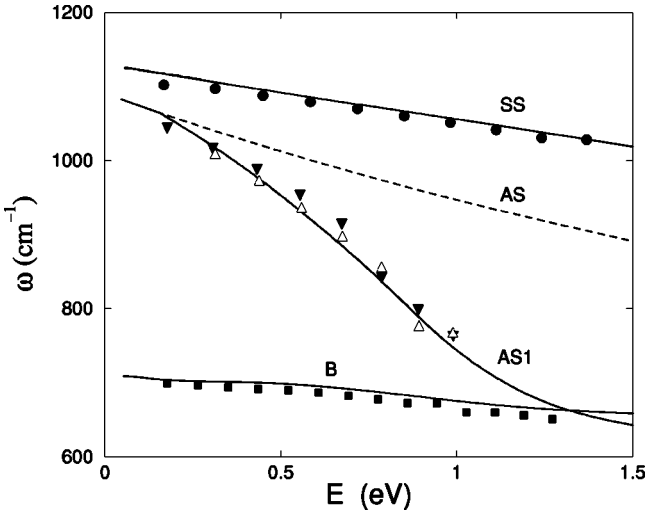

FIG. 8. The frequencies of the classical periodic orbits of the symmetric stretch (SS), the bending (B), and two types of antisymmetric stretching (AS, AS1) families. The corresponding quantum mechanical frequencies of the overtone progressions $(v_1,0,0)$, $(0,v_2,0)$, and $(0,0,v_3)$ are represented by the black symbols. The open triangles indicate the frequencies for the $(1,0,v_3-1)$ states, which are almost degenerate with the $(0,0,v_3)$ states. For more details see the text.

erate pairs with bending excitation, like, e.g., (0,2,5) and (1,2,4) with an energy gap of 31 cm^{-1}.

C. Comparison with experimental energies

The microwave and infrared spectroscopy of ozone is thoroughly investigated.[74,84] The energies of more than 70 vibrational states of $^{16}O_3$, 35 states of $^{18}O_3$, and 60 states of other isotopomers are known and form a solid basis for assessing the accuracy of our PES, at least its bound region. In Table III we compare 68 calculated vibrational energies of $^{16}O_3$ with the experimental energies; only the states up to (6,0,0) are listed here. The main body of measured data are taken from direct high-resolution experiments and have been compiled by Tyuterev *et al.* (Table 2 of Ref. 30). Some additional energies have been determined by ''dark state'' analysis (Table 3 of Ref. 30) and through perturbations (Fig. 14 of Ref. 85). A small set of additional data at high excitation energies has been obtained through Raman spectroscopy by Chang *et al.*;[86] they do not have, however, the precision of the high-resolution spectroscopic data.

The agreement is very good—especially if one bears in mind that the PES has not been scaled or otherwise modified. With an error of 2.4 cm^{-1} the bending frequency is reproduced worst. Therefore, as more and more quanta of the bending progression are excited the deviation gradually increases being 11.7 cm^{-1} for (0,8,0). A slight scaling of the PES in this coordinate probably would improve the general accuracy. In addition to the energies in Table III, the energies for states (3,0,4) and (5,0,2) are known from the work of Chang *et al.*[86] The calculated energies (in cm^{-1}) are 6921.6 (6927) and 7220.8 (7227), respectively, with the experimental values given in parentheses. Moreover, Chang *et al.* measured the energies of the high overtone states $(v_1,0,0)$ with $v_1=7-10$. The corresponding calculated energies are (in cm^{-1}): 7547 (7555), 8588 (8598), 9619 (9632), and 10 642 (10 650) with the experimental energies again given in parentheses. The discrepancies are all in the range of merely 10 cm^{-1}. In general, the deviation increases with energy. The root-mean-square error is 5 cm^{-1} and the mean deviation is 4 cm^{-1}. The 68 states given in Table III, and the states (3,0,4), (5,0,2), (0,0,7) (see below), and (7,0,0) are taken into account for calculating these deviations; all these states are bound states. The few additional states quoted by Chang *et al.*[86] are resonance states.

Very recently, Wenz *et al.*[87] identified three additional vibrational states at high energies and analyzed them. The measured energies (in cm^{-1}) and the experimental assignments are: 6568.1 (0,0,7), 6570.5 (1,0,6), and 6587.0 (2,0,5). As stated by Wenz *et al.*, due to severe congestion the assignment was difficult and problematic at these high energies. The state, which in the calculation is interpreted as (0,0,7) has an energy of 6557.2 cm^{-1}, which agrees quite well with the measured energy. Because of mixing with a nearby state, probably (4,2,1), this state is highly mixed in the calculation as has been discussed above. In the calculations there are two states which could be interpreted as (1,0,6). The first is slightly lower than (0,0,7) and has an energy of 6553.4 cm^{-1}, which is by 17.1 cm^{-1} in disagreement with the experimental value. The other one has an energy of 6620.9 cm^{-1}, which is 50.4 cm^{-1} higher than the experimentally assigned (1,0,6) level. Because this disagreement is much larger than encountered for all the lower vibrational states, we believe that this level is not related to the level assigned as (1,0,6) by Wenz *et al.* However, the calculated state (4,2,1) is slightly above (0,0,7) and has an energy of 6576.2 cm^{-1}, which agrees quite well with the experimental energy of 6570.5 cm^{-1}. Thus, this state is another alternative for the state interpreted as (1,0,6) by Wenz *et al.* In the calculation there is no state in the vicinity of (0,0,7) which could be assigned as (2,0,5). A state with an energy of 6602.8 cm^{-1} is the only reasonable candidate to correspond to the observed level at 6587.0 cm^{-1}. Its wave function is rather clear and has the assignment (3,5,0).

These difficulties in establishing undisputable relationships between the three measured energies in the vicinity of (0,0,7) and the calculated energies indicate the general dilemma of comparing measured and calculated energies of highly excited ozone. Due to mixings the wave functions are less and less clear and assignments become questionable—despite the extremely small density of states. Unlike HOCl[88,89] or HCP,[90] in ozone all three modes are coupled and a decoupling based on an adiabatic separation is not obvious.

The energies of the other isotopomers (Tables IV and V) are equally well reproduced. Because the experimentally available data do not extend to energies as high as for $^{16}O_3$, the root-mean-square errors and the mean deviations are smaller than for $^{16}O_3$.

The rotational constants for the vibrational ground state and the lowest 12 excited states have been determined from energy differences for total angular momenta $J=0$ and 2 including Coriolis coupling. The results are presented and compared with the experimental data as collected in Ref. 74

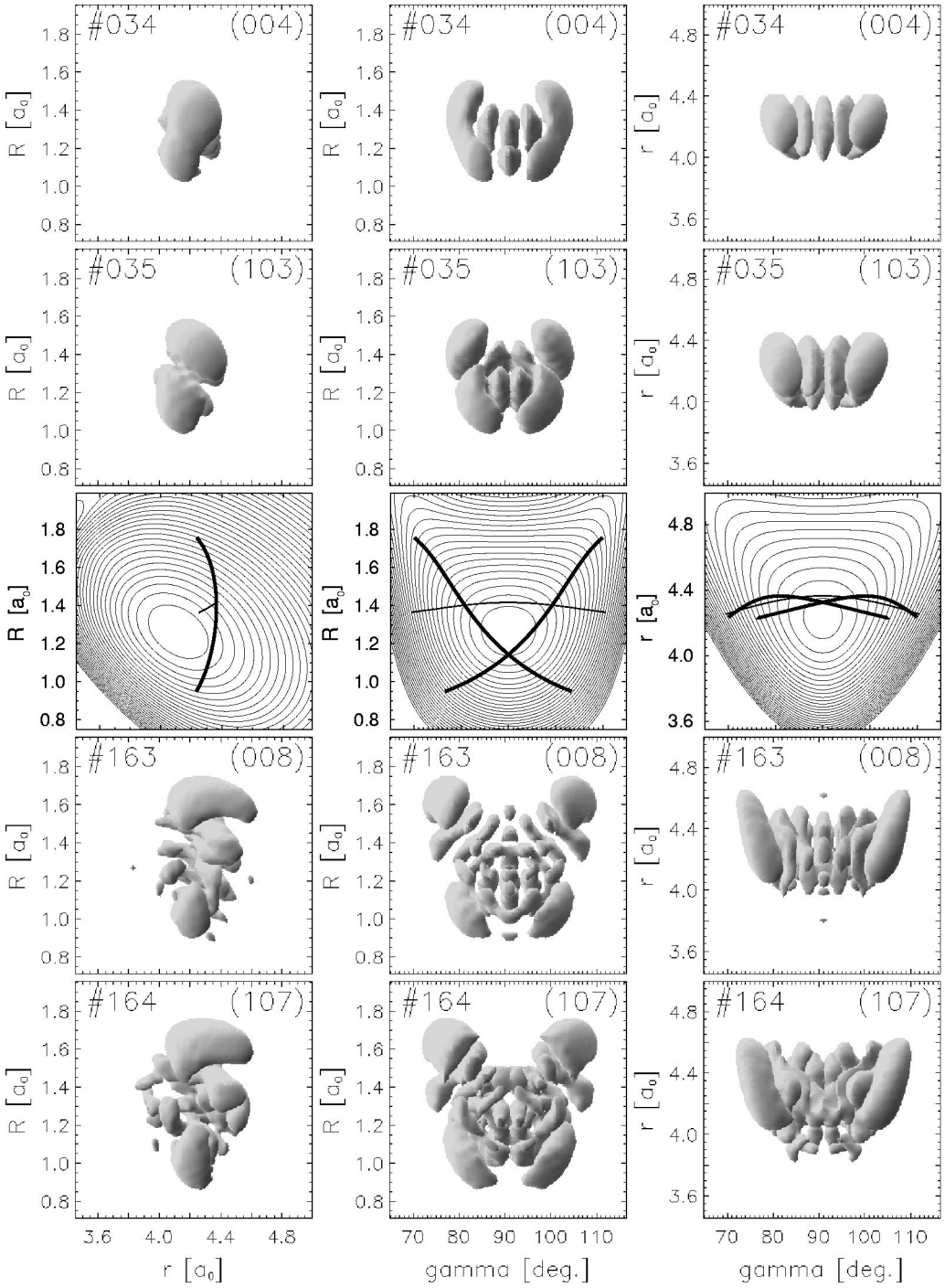

FIG. 9. Wave functions of the two almost degenerate states at the bottom of the $[v_2=0,P=4]$ and [0,8] polyads. The two-dimensional cuts through the PES are shown in the middle part of the figure. They contain the AS (thin lines) and the two AS1 (thick lines) classical periodic orbits for $E=1.1$ eV. For more details see Fig. 5.

in Table VI. They are in excellent agreement with the measured values and reproduce the correct trends as function of excitation.

Finally, we compare in Table VII the calculated and measured vibrational energies and rotational constants for the $^{16}O_2$ fragment. They also agree well with the experimental values. The corresponding data for all other isotopes of O_2 can be obtained electronically.[49]

V. PERIODIC ORBITS

It is well known that classical periodic orbits (PO's) are very helpful in interpreting quantum mechanical wave functions.[76,90,97–99] Periodic orbits and their stability properties reflect the structure of the classical phase space, i.e., regions where the classical motion is regular or chaotic. In particular, by following the PO's with total energy and constructing continuation/bifurcation diagrams one obtains a

TABLE III. Comparison of calculated and measured term values for $^{16}O_3$.

(v_1,v_2,v_3)	E^a	ΔE^a	Ref.	(v_1,v_2,v_3)	E^a	ΔE^a	Ref.
(0,1,0)	698.5	2.4	30	(2,3,0)[b]	4 240.3	6.4	30
(0,0,1)	1 043.9	−1.8	30	(3,0,1)	4 248.9	1.3	30
(1,0,0)	1 101.9	1.2	30	(0,2,3)	4 344.4	2.3	30
(0,2,0)	1 394.3	5.0	30	(4,0,0)[b]	4 365.8	4.5	30
(0,1,1)[b]	1 726.0	0.5	30	(1,2,2)[b]	4 387.0	3.5	30
(1,1,0)	1 792.4	3.9	30	(2,2,1)	4 504.6	3.5	30
(0,0,2)	2 060.6	−2.7	30	(3,2,0)[bc]	4 640.0	3.8	30
(0,3,0)	2 088.1	6.9	30	(0,1,4)[c]	4 629.4	3.5	30
(1,0,1)	2 111.3	−0.5	30	(1,1,3)	4 655.9	3.0	30
(2,0,0)	2 199.0	2.2	30	(1,4,1)[d]	4 778.2	5.0	85
(0,2,1)	2 404.8	3.1	30	(2,1,2)	4 781.7	1.8	30
(1,2,0)	2 481.1	5.5	30	(3,1,1)[e]	4 893.9	3.4	30
(0,1,2)	2 726.3	−0.2	30	(0,0,5)[f]	4 916.6	2.6	30
(0,4,0)[b]	2 780.2	7.7	30	(1,0,4)	4 919.3	3.3	30
(1,1,1)	2 783.2	2.0	30	(1,3,2)[b]	5 031.1	7.4	30
(2,1,0)	2 881.7	4.5	30	(2,0,3)	5 077.6	−0.5	30
(0,0,3)	3 048.6	−2.5	30	(3,0,2)	5 170.4	0.0	86
(0,3,1)	3 081.3	4.9	30	(0,2,4)[b]	5 261.1	5.8	30
(1,0,2)	3 084.5	−0.8	30	(1,2,3)	5 285.9	5.3	30
(1,3,0)	3 168.1	5.8	30	(3,3,0)[b]	5 303.3	7.2	30
(2,0,1)	3 186.3	0.1	30	(4,0,1)	5 305.6	2.2	30
(3,0,0)	3 286.7	3.2	30	(5,0,0)	5 435.7	7	86
(0,2,2)	3 388.7	2.2	30	(0,1,5)[g]	5 512.7	6.1	30
(1,2,1)	3 452.3	3.5	30	(0,8,0)[b]	5 516.1	11.6	30
(0,5,0)[c]	3 470.0	8.4	85	(1,1,4)	5 534.7	6.2	30
(0,1,3)	3 698.3	0.0	30	(3,2,1)[h]	5 555.1	7	86
(1,1,2)	3 737.7	1.7	30	(2,1,3)	5 694.6	2.7	30
(2,1,1)	3 847.6	2.3	30	(4,2,0)[b]	5 695.3	6.3	30
(1,4,0)[d]	3 851.6	6.9	85	(0,0,6)[b]	5 758.7	7.8	30
(3,1,0)	3 961.8	4.9	30	(3,1,2)[b]	5 809.2	3.4	30
(0,0,4)	4 002.1	−0.8	30	(1,0,5)	5 776.5	7.3	30
(1,0,3)	4 021.4	0.4	30	(2,0,4)	5 993.7	3	86
(1,3,1)	4 118.0	4.1	30	(4,0,2)	6 202.5	2	86
(2,0,2)	4 142.1	−0.7	30	(6,0,0)	6 496.0	10	86

[a]Energies are given in cm^{-1}. ΔE = obs.−calc.
[b]From "dark state" analysis.
[c]Mixing between (3,2,0) and (0,1,4).
[d]Observed through perturbations.
[e]Wave function not clearly assignable; probably mixing with (0,0,5).
[f]Wave function not clearly assignable; probably mixing with (3,1,1).
[g]Wave function not clearly assignable; probably mixing with (3,2,1).
[h]Wave function not clearly assignable; probably mixing with (0,1,5).

global view of how the dynamics change with energy. As energy increases nonlinear effects like bifurcations may occur and these bifurcations in the classical phase space may leave pronounced marks in the development of the quantum wave functions with increasing excitation.[90] In previous publications[99,100] the methods that we use to locate PO's, to continue them with total energy, and to construct continuation/bifurcation diagrams are fully described. In numerous applications it has been found useful to plot the frequencies of PO's ($\omega = 2\pi/T$) as function of total energy and to compare these classical frequencies with the quantum mechanical counterparts.

In Fig. 8 we show the frequencies of the three principal families of PO's, i.e., the symmetric stretch (SS), the antisymmetric stretch (AS), and the bend (B). The symbols denote the differences of adjacent quantum energy levels in a particular progression, for example, $E_{(v_1,0,0)} - E_{(v_1-1,0,0)}$; they are plotted at the energy of the lower level. The frequency of the SS mode decreases almost linearly with energy and agrees well with the quantum mechanical frequency of the symmetric stretch mode. The frequency of the bending mode depends only very slightly on E and also agrees with the quantum frequency in this mode. Even the slightly indicated curvature seen in the quantum results is nicely reproduced. Without showing results, the SS and B PO's scar the corresponding wave functions, $(v_1,0,0)$ and $(0,v_2,0)$, respectively. They are mostly stable and only occasionally become single unstable (instability in one degree of freedom) in some energy intervals; however, they never become highly unstable and remain stable even above the dissociation limit.

Most interesting is the behavior of the asymmetric stretching mode, AS. Its frequency is only slightly more anharmonic than the frequency of the SS mode. However, no quantum wave function is scarred by the AS PO's, that is, the AS periodic orbits have no counterpart in quantum mechanics. An example of a AS-type PO is depicted in Fig. 9; it is symmetric with respect to $\gamma = 90°$. Although the energy is quite high, R and r remain almost constant along the trajec-

TABLE IV. Comparison of calculated and measured term values for $^{18}O_3$.

(v_1,v_2,v_3)	E^a	ΔE^a	Ref.	(v_1,v_2,v_3)	E^a	ΔE^a	Ref.
(0,1,0)	659.3	2.2	91	(2,0,1)	3 012.5	0.0	91
(0,0,1)	986.6	−1.8	91	(0,2,2)[b]	3 206.6	1.2	85
(1,0,0)	1 040.4	1.2	91	(1,2,1)	3 265.7	3.5	85
(0,2,0)	1 316.0	4.7	91	(0,1,3)	3 502.6	−0.4	85
(0,1,1)	1 613.3	0.4	91	(1,1,2)[b]	3 540.5	1.4	85
(1,1,0)	1 692.5	3.7	91	(3,1,0)[b]	3 742.6	4.1	85
(0,0,2)	1 949.1	−2.6	91	0,0,4)[b]	3 794.2	−1.3	85
(1,0,1)	1 996.5	−0.5	91	(1,0,3)	3 813.7	−0.3	85
(2,0,0)	2 076.3	2.1	91	(3,0,1)	4 018.2	1.1	85
(0,2,1)	2 273.0	3.0	91	(0,2,3)	4 115.5	1.8	85
(1,2,0)	2 342.9	5.4	91	(3,2,0)[b]	4 378.7	6.6	85
(0,1,2)	2 579.4	−0.4	91	(0,1,4)[b]	4 396.4	1.5	85
(0,4,0)[b]	2 624.4	7.3	91	(1,1,3)	4 416.6	2.3	85
(1,1,1)	2 632.4	1.8	91	(3,1,1)[b]	4 643.0	3.0	85
(2,1,0)	2 721.6	4.3	91	(0,0,5)	4 665.4	1.4	85
(0,0,3)	2 886.6	−2.7	91	(1,0,4)[b]	4 672.0	2.1	85
(1,0,2)	2 921.0	−1.0	91	(2,0,3)	4 809.6	−1.0	85
(1,3,0)[b]	2 992.1	6.9	91				

[a]Energies are given in cm^{-1}. ΔE = obs.−calc.
[b]Observed through perturbations.

tory; only the angle varies over a large range. The AS PO's avoid the dissociation path and stay in the inner region of the potential. Therefore, their frequencies are only moderately anharmonic.

The wave functions of the $(0,0,v_3)$ states follow antisymmetric stretch PO's which come into existence at an early bifurcation of the AS family of orbits; they will be termed AS1 in what follows. The new PO's initially have the same period as the AS ones, however, their frequency decreases much faster with energy. This is typical for a normal- to local-mode transition;[101] for a recent investigation of such a bifurcation see Ref. 102. The AS PO's become unstable at the bifurcation, but may become stable again at higher energies, whereas the new PO's are stable. Actually, there are two different AS1 PO's for each energy. One is the reflection of the other one at the plane defined by $\gamma=90°$; their frequencies are obviously identical. In contrast to the AS PO's, the AS1 trajectories do follow the reaction path (Fig. 9) and therefore they are highly anharmonic. Plotting the AS1 PO's in the two bond coordinates R_1 and R_2 clearly shows their local-mode character. As indicated by the trajectories as well as the good agreement between the quantal and the classical frequencies, it are the AS1 PO's which scar the $(0,0,v_3)$ and the $(1,0,v_3-1)$ wave functions. The AS1 PO's continue above the dissociation threshold and eventually become single unstable with the instability increasing with energy. The change of the slope around 1 eV seems to indicate a saddle node bifurcation as has been observed, e.g., for HOCl.[89]

The analysis of the classical PO's is in accord with the quantum mechanical picture in (i) that all three important families of PO's—SS, B, and AS1—can be followed to high energies without any problems and (ii) that there are no bifurcations in the bound-state energy region, except the very early AS/AS1 bifurcation. A saddle-node bifurcation, for example, would lead to more drastic changes of the wave functions, which are not observed. The absence of bifurcations is probably the consequence of the mismatch of the three frequencies over the entire energy range from the bottom of the well to the dissociation threshold. In future work we will analyze in more detail the PO's around the threshold and their changes with isotopic substitution. Any differences in the classical phase spaces for symmetric and nonsymmetric isotopes, ABA and ABB, for example, may have consequences for the lifetimes of these complexes and therefore for the rate coefficients for ozone formation.

VI. SUMMARY

(1) An accurate potential energy surface (PES) for the lowest state of ozone has been constructed. The electronic structure calculations are performed at the multireference configuration interaction level with complete active space self-consistent-field reference functions. The correlation consistent polarized quadruple zeta atomic basis functions are employed. The PES is global, that is, it covers the three open minima, each having C_{2v} symmetry, the ring minimum with D_{3h} symmetry, and the product channels. The equilibrium coordinates, the dissociation energy, and other critical values agree well with experimental data or the results of previous calculations.

(2) The ring minimum belongs to a different electronic state with $^1A'$ symmetry. It is located well above the $O+O_2$ asymptote. Due to the conical intersection between the two $^1A'$ states a high crest surrounds the ring minimum with the consequence, that it very likely does not influence the kinetics of ozone formation and dissociation at low and intermediate temperatures.

(3) Towards the dissociation channel the PES has a sharp, edgelike behavior with a tiny barrier at intermediate O–O separations. The height of this barrier depends drastically on the atomic basis set in the electronic structure calculations. For the largest basis used, cc-pV5Z, the barrier is located *under* the $O+O_2$ asymptote; nevertheless, the slope

TABLE V. Comparison of calculated and measured term values for several isotopes of O_3.

(v_1,v_2,v_3)	E^a	ΔE^a	Ref.	(v_1,v_2,v_3)	E^a	ΔE^a	Ref.
	$^{16}O^{17}O^{17}O$				$^{17}O^{17}O^{17}O$		
(0,0,1)	1 019.3	−1.8	92	(0,0,1)	1 014.0	−1.8	74
(1,0,0)	1 079.0	1.2	92	(1,0,0)	1 069.7	1.2	74
	$^{17}O^{16}O^{17}O$						
(0,0,1)	1 031.9	−1.8	93				
(1,0,0)	1 085.6	1.1	93				
	$^{16}O^{16}O^{17}O$				$^{16}O^{17}O^{16}O$		
(0,1,0)	690.0	2.4	74	(0,1,0)	694.7	2.4	74
(0,0,1)	1 037.2	−1.8	74	(0,0,1)	1 026.2	−1.8	74
(1,0,0)	1 094.5	1.2	74	(1,0,0)	1 086.6	1.2	74
(0,0,2)	2 046.7	1.2	94	(0,0,2)	2 026.5	2.1	94
(1,0,1)	2 099.5	−0.6	94	(1,0,1)	2 078.8	−0.5	94
(2,0,0)	2 183.3	−1.2	94	(2,0,0)	2 168.2	−0.5	94
	$^{16}O^{18}O^{16}O$				$^{16}O^{18}O^{18}O$		
(0,1,0)	690.6	5.7	74	(0,1,0)	675.2	2.3	74
(0,0,1)	1 009.8	−1.3	74	(0,0,1)	995.6	−1.7	95
(1,0,0)	1 072.6	1.7	74	(1,0,0)	1 059.6	1.1	95
(1,0,1)	2 049.4	0	74	(0,1,1)	1 656.2	0.5	95
(1,1,1)	2 715.6	2.4	95	(1,0,1)	2 028.4	−0.8	74
(0,0,3)	2 954.7	−2.3	95	(1,1,1)	2 679.0	1.6	95
(2,0,1)	3 095.0	0.7	95	(0,0,3)	2 905.4	−2.2	95
(0,1,3)	3 600.3	0.1	95	(2,0,2)	3 055.4	0.3	95
(1,0,3)	3 903.7	0.6	95	(1,0,3)	3 883.8	−0.8	95
(0,0,5)	4 762.0	3.1	95	(1,1,3)	4 500.4	1.7	95
	$^{16}O^{16}O^{18}O$				$^{18}O^{16}O^{18}O$		
(0,1,0)	682.2	2.4	74	(0,1,0)	665.4	2.7	74
(0,0,1)	1 029.8	−1.7	74	(0,0,1)	1 020.8	−1.4	74
(1,0,0)	1 089.3	1.1	74	(1,0,0)	1 070.7	1.5	74
(0,1,1)	1 696.2	0.7	95	(0,1,1)	1 670.8	0.9	95
(1,0,1)	2 091.2	−0.9	95	(1,0,1)	2 060.3	−0.2	95
(2,0,0)	2 170.4	2.6	95	(1,1,1)	2 701.0	2.3	95
(1,1,1)	2 747.0	1.8	95	(0,0,3)	2 982.7	−2.2	95
(0,0,3)	3 000.9	−2.0	95	(2,0,1)	3 107.2	0.3	95
(1,0,2)	3 062.0	−1.4	95	(0,1,3)	3 600.9	0.9	95
(2,0,1)	3 148.0	0.1	95	(1,0,3)	3 935.1	0.5	95
				(1,1,3)	4 540.2	3.1	95
				(0,0,5)	4 811.8	2.4	95

[a]Energies are given in cm^{-1}. ΔE = obs.−calc.

TABLE VI. Comparison of calculated and measured rotational constants (in cm^{-1}) for the 13 lowest states of $^{16}O_3$.

(v_1,v_2,v_3)	A	ΔA^a	B	ΔB^a	C	ΔC^a
(0,0,0)	3.542	0.012	0.4416	0.0036	0.3920	0.0028
(0,1,0)	3.593	0.014	0.4389	0.0051	0.3883	0.0041
(0,0,1)	3.486	0.014	0.4351	0.0061	0.3819	0.0091
(1,0,0)	3.542	0.014	0.4371	0.0057	0.3916	0.0009
(0,2,0)	3.647	0.015	0.4362	0.0075	0.3846	0.0055
(0,1,1)	3.537	0.015	0.4337	0.0061	0.3800	0.0084
(1,1,0)	3.594	0.016	0.4343	0.0071	0.3874	0.0029
(0,0,2)	3.438	0.010	0.4305	0.0070	0.3766	0.0113
(1,0,1)	3.486	0.015	0.4312	0.0073	0.3801	0.0081
(2,0,0)	3.538	0.021	0.4327	0.0073	0.3905	−0.0004
(0,2,1)	3.591	0.014	0.4329	0.0055	0.3785	0.0075
(1,2,0)	3.652	0.014	0.4320	0.0140	0.3838	0.0101
(0,1,2)	3.485	0.015	0.4253	0.0105	0.3707	0.0147

[a]obs.−calc., experimental values from Ref. 74, Table 10.

TABLE VII. Comparison of calculated and measured vibrational energies and rotational constants (in cm^{-1}) for $^{16}O_2$.

v	E	ΔE^a	B	ΔB^a
0	0.00	0.0	1.432	0.006
1	1553.45	3.0	1.417	0.005
2	3084.78	4.2	1.401	0.005
3	4593.93	4.7	1.386	0.005
4	6080.79	4.2	1.370	0.005
5	7545.25	3.1	1.355	0.005
6	8987.21	1.5	1.340	0.004
7	10 406.54	−0.1	1.324	0.004
8	11 803.15	−1.7	1.309	0.004
9	13 176.89	−3.1	1.294	0.004
10	14 527.62	−4.1	1.278	0.004
11	15 855.09	−4.5	1.263	0.003
12	17 158.97	−4.0	1.249	0.002
13	18 438.70	−2.2	1.235	0.000
14	19 693.54	1.7	1.221	−0.002

[a]obs.−calc., experimental values from Ref. 96, Table XIII.

of the PES still changes abruptly in the region of the barrier. The transition state (TS) is very tight with the lowest TS frequency being 276 cm^{-1}.

(4) The calculated transition energies for $^{16}O_3$ agree very well with the experimental values. This includes 72 vibrational states up to an energy of about 6500 cm^{-1} with respect to the lowest state or slightly more than 85% of the calculated dissociation energy. The root-mean-square deviation is 5 cm^{-1} and the mean deviation is 4 cm^{-1}. The agreement with the experimental transition energies is equally good for all the other isotopes, for which data are available. Also, the vibrational energies of O_2 are reproduced with similar accuracy.

(5) Most states up to an energy of 6000 cm^{-1} or 80% of the (calculated) dissociation energy can be unambiguously assigned. At higher energies more and more wave functions have a complicated nodal structure, caused by mixings with other states, and cannot be assigned. The symmetric stretching and the bending states can be followed without problems to energies well above the dissociation threshold. The states of the antisymmetric stretch mode also can be followed to the threshold, although the higher overtones show severe mixing. The assignability of a substantial number of states even near the dissociation threshold indicates a high degree of regularity.

(6) In accord with the assignability of the wave functions of the $(v_1,0,0)$ and $(0,v_2,0)$ progressions, the classical periodic orbits (PO's) belonging to the symmetric stretch and bend families can be followed up to high energies above the threshold. The antisymmetric stretch PO's show an early bifurcation at very low energies. The quantum wave functions of the $(0,0,v_3)$ progression follow the bifurcating antisymmetric stretch PO's, whose frequency drastically decreases with energy. Both, the antisymmetric stretch wave functions and the corresponding PO's exhibit a local-mode behavior at high excitation energies.

ACKNOWLEDGMENTS

Financial support by the Deutsche Forschungsgemeinschaft through the Sonderforschungsbereich 357 ''Molekulare Mechanismen Unimolekularer Reaktionen'' and the Fonds der Chemischen Industrie is gratefully acknowledged. S.C.F. and R.S. are grateful to the Alexander von Humboldt-Stiftung for a travel grant and P.F.-L. thanks the Alexander von Humboldt-Stiftung for a stipend. R.S. acknowledges many stimulating discussions with S. Yu. Grebenshchikov. The calculations have been performed on the workstation clusters of the MPI für Strömungsforschung (Department of Nonlinear Dynamics) and the Gesellschaft für Wissenschaftliche Datenverarbeitung Göttingen (GWDG).

[1] B. J. Finlayson-Pitts and J. N. Pitts, Jr., *Atmospheric Chemistry* (Wiley, New York, 1986).
[2] R. P. Wayne, Atmos. Environ. **21**, 1683 (1987).
[3] R. P. Wayne, *Chemistry of Atmospheres*, 2nd ed. (Oxford University Press, Oxford, 1991).
[4] H. Hippler, R. Rahn, and J. Troe, J. Chem. Phys. **93**, 6560 (1990).
[5] D. Krankowsky and K. Mauersberger, Science **274**, 1324 (1996).
[6] D. Krankowsky, F. Bartecki, G. G. Klees, K. Mauersberger, K. Schellenbach, and J. Stehr, Geophys. Res. Lett. **22**, 1713 (1995).
[7] J. C. Johnson and M. H. Thiemens, J. Geophys. Res. **102**, 25395 (1997).
[8] F. W. Irion, M. R. Gunson, C. P. Rinsland, Y. L. Yung, M. C. Abrams, A. Y. Chang, and A. Goldman, Geophys. Res. Lett. **23**, 2377 (1996).
[9] M. H. Thiemens and T. Jackson, Geophys. Res. Lett. **15**, 639 (1988).
[10] K. Mauersberger, B. Erbacher, D. Krankowsky, J. Günther, and R. Nickel, Science **283**, 370 (1999).
[11] S. Wolf, M. Bitter, D. Krankowsky, and K. Mauersberger, J. Chem. Phys. **113**, 2684 (2000).
[12] C. Janssen, J. Guenther, K. Mauersberger, and D. Krankowsky, Phys. Chem. Chem. Phys. **3**, 4718 (2001).
[13] R. E. Weston, Jr., Chem. Rev. **99**, 2115 (1999).
[14] M. R. Wiegell, N. W. Larsen, T. Pedersen, and H. Egsgaard, Int. J. Chem. Kinet. **29**, 745 (1997).
[15] B. C. Hathorn and R. A. Marcus, J. Chem. Phys. **111**, 4087 (1999).
[16] B. C. Hathorn and R. A. Marcus, J. Chem. Phys. **113**, 9497 (2000).
[17] Y. Q. Gao and R. A. Marcus, J. Chem. Phys. **116**, 137 (2002).
[18] Y. Q. Gao and R. A. Marcus, Science **293**, 259 (2001).
[19] R. Siebert, R. Schinke, and M. Bittererová, Phys. Chem. Chem. Phys. **3**, 1795 (2001).
[20] T. Baer and W. L. Hase, *Unimolecular Reaction Dynamics* (Oxford University Press, Oxford, 1996).
[21] R. Schinke, *Photodissociation Dynamics* (Cambridge University Press, Cambridge, 1993).
[22] T. Müller, S. S. Xantheas, H. Dachsel, R. J. Harrison, J. Nieplocha, R. Shepard, G. S. Kedziora, and H. Lischa, Chem. Phys. Lett. **293**, 72 (1998).
[23] A. Banichevich, S. D. Peyerimhoff, and F. Grein, Chem. Phys. **178**, 155 (1993).
[24] P. Borowski, M. Fülscher, P. Å. Malmquist, and B. O. Roos, Chem. Phys. Lett. **237**, 195 (1995).
[25] G. J. Atchity and K. Ruedenberg, Theor. Chem. Acc. **96**, 176 (1997).
[26] G. J. Atchity, K. Ruedenberg, and A. Nanayakkara, Theor. Chem. Acc. **96**, 195 (1997).
[27] D. Xie, H. Guo, and K. A. Peterson, J. Chem. Phys. **112**, 8378 (2000).
[28] K. Yamashita, K. Morokuma, F. Le Quéré, and C. Leforestier, Chem. Phys. Lett. **191**, 515 (1992).
[29] A. Gross and G. D. Billing, Chem. Phys. **217**, 1 (1997).
[30] Vl. G. Tyuterev, S. Tashkun, P. Jensen, A. Barbe, and T. Cours, J. Mol. Spectrosc. **198**, 57 (1999).
[31] Vl. G. Tyuterev, S. Tashkun, D. W. Schwenke, P. Jensen, T. Cours, A. Barbe, and M. Jacon, Chem. Phys. Lett. **316**, 271 (2000).
[32] T. H. Dunning, Jr., J. Chem. Phys. **90**, 1007 (1989).
[33] T. Müller, M. Dallos, H. Lischka, Z. Dubrovay, and P. G. Szalay, Theor. Chem. Acc. **105**, 227 (2001).
[34] H.-J. Werner and P. J. Knowles, J. Chem. Phys. **82**, 5053 (1985).
[35] P. J. Knowles and H.-J. Werner, Chem. Phys. Lett. **115**, 259 (1985).
[36] H.-J. Werner and P. J. Knowles, J. Chem. Phys. **89**, 5803 (1988).
[37] P. J. Knowles and H.-J. Werner, Chem. Phys. Lett. **145**, 514 (1988).
[38] S. R. Langhoff and E. R. Davidson, Int. J. Quantum Chem. **8**, 61 (1974).
[39] P. G. Szalay and R. J. Bartlett, Chem. Phys. Lett. **214**, 481 (1993).
[40] P. G. Szalay and R. J. Bartlett, J. Chem. Phys. **103**, 3600 (1995).
[41] P. Fleurat-Lessard, R. Siebert, R. Schinke, and N. Halberstadt (unpublished).
[42] MOLPRO98 is a package of *ab initio* programs written by H.-J. Werner and P. J. Knowles, with contributions from J. Almlöf, R. D. Amos, A. Berning, *et al.*
[43] W. A. Goddard III, T. H. Dunning, Jr., W. J. Hunt, and P. J. Hay, Acc. Chem. Res. **6**, 368 (1973).
[44] S. Shih, R. J. Buenker, and S. D. Peyerimhoff, Chem. Phys. Lett. **28**, 463 (1974).
[45] P. J. Hay, T. H. Dunning, Jr., and W. A. Goddard III, J. Chem. Phys. **62**, 3912 (1975).
[46] S. S. Xantheas, G. J. Atchity, S. T. Elbert, and K. Ruedenberg, J. Chem. Phys. **94**, 8054 (1991).
[47] G. J. Atchity and K. Ruedenberg, Theor. Chem. Acc. **96**, 205 (1997).
[48] G.-s. Wu, G. C. Schatz, D. Lendvay, D.,-C. Fang, and L. B. Harding, J. Chem. Phys. **113**, 3150 (2000).
[49] See EPAPS Document No. E-JCPSA6-116-010221 for the calculated energies, plots of the PES in terms of coordinates preserving D_{3h} symmetry, plots of the wave functions for the bound states of ozone, plots of the wave functions of states (3,1,1) and (0,0,5), and the vibrational energies and rotational constants of the different isotopes of O_2. This document may be retrieved via the EPAPS homepage (http://www.aip.org/pubservs/epaps.html) or from ftp.aip.org in the directory /epaps/. See the EPAPS homepage for more information.

[50] J. N. Murrell, S. Carter, S. C. Farantos, P. Huxley, and A. J. C. Varandas, *Molecular Potential Energy Functions* (Wiley, Chichester, 1984).
[51] M. W. Chase, Jr., C. A. Davies, J. R. Downey, Jr., D. J. Frurip, R. A. McDonald, and A. N. Syverud, J. Phys. Chem. Ref. Data **14**, 1 (1985).
[52] J. L. Gole and R. N. Zare, J. Chem. Phys. **57**, 5331 (1972).
[53] T. J. Lee, Chem. Phys. Lett. **169**, 529 (1990).
[54] J. Ivanic, G. J. Atchity, and K. Ruedenberg, J. Chem. Phys. **107**, 4307 (1997).
[55] N. Sukumar and S. D. Peyerimhoff, Mol. Phys. **95**, 61 (1998).
[56] R. Plass, K. Egan, C. Collazo-Davila, D. Grozea, E. Landree, L. D. Marks, and M. Gajdardziska-Josifovska, Phys. Rev. Lett. **81**, 4891 (1998).
[57] R. Siebert and R. Schinke (unpublished).
[58] M. R. Wall and D. Neuhauser, J. Chem. Phys. **102**, 8011 (1995).
[59] V. A. Mandelshtam and H. S. Taylor, J. Chem. Phys. **102**, 7390 (1995).
[60] T. P. Grozdanov, V. A. Mandelshtam, and H. S. Taylor, J. Chem. Phys. **103**, 7990 (1995).
[61] G. Jolicard and E. J. Austin, Chem. Phys. Lett. **121**, 106 (1985).
[62] G. Jolicard and E. J. Austin, Chem. Phys. **103**, 295 (1986).
[63] U. V. Riss and H.-D. Meyer, J. Phys. B **24**, 4503 (1993).
[64] R. Kosloff, Annu. Rev. Phys. Chem. **45**, 145 (1994).
[65] V. A. Mandelshtam, T. P. Grozdanov, and H. S. Taylor, J. Chem. Phys. **103**, 10074 (1995).
[66] J. Echave and D. C. Clary, Chem. Phys. Lett. **190**, 225 (1992).
[67] Z. Bačić and J. C. Light, Annu. Rev. Phys. Chem. **40**, 469 (1989).
[68] S. Schmatz, P. Botschwina, J. Hauschildt, and R. Schinke, J. Chem. Phys. **114**, 5233 (2001).
[69] V. A. Mandelshtam and H. S. Taylor, Phys. Rev. Lett. **78**, 3274 (1997).
[70] V. A. Mandelshtam and H. S. Taylor, J. Chem. Phys. **106**, 5085 (1997).
[71] M. S. Child and L. Halonen, Adv. Chem. Phys. **57**, 1 (1984).
[72] M. S. Child, Acc. Chem. Res. **18**, 45 (1985).
[73] F. Péarez-Bernal, J. M. Arias, A. Frank, R. Lemus, and R. Bijker, J. Mol. Spectrosc. **184**, 1 (1997).
[74] J.-M. Flaud and R. Bacis, Spectrochim. Acta, Part A **54**, 3 (1998).
[75] J.-M. Flaud, A. Barbe, C. Camy-Peyret, and J. J. Plateaux, J. Mol. Spectrosc. **177**, 34 (1996).
[76] M. Joyeux, S. C. Farantos, and R. Schinke, J. Phys. Chem. A (to be published).
[77] M. E. Kellman, J. Chem. Phys. **83**, 3843 (1985).
[78] M. S. Child, *Semiclassical Mechanics with Molecular Applications* (Clarendon, Oxford, 1991).
[79] L. Halonen, Adv. Chem. Phys. **104**, 41 (1998).
[80] R. T. Lawton and M. S. Child, Mol. Phys. **37**, 1799 (1979).
[81] R. T. Lawton and M. S. Child, Mol. Phys. **44**, 709 (1981).
[82] M. J. Davis and E. J. Heller, J. Chem. Phys. **75**, 246 (1981).
[83] E. L. Sibert, J. T. Hynes, and W. P. Reinhardt, J. Chem. Phys. **77**, 3595 (1982).
[84] J. I. Steinfeld, S. M. Adler-Golden, and J. W. Gallagher, J. Phys. Chem. Ref. Data **16**, 911 (1987).
[85] A. Chichery, A. Barbe, and V. G. Tyuterev, J. Mol. Spectrosc. **206**, 14 (2001).
[86] B.-Y. Chang, C.-Y. Kung, C. Kittrell, C.-W. Hsiao, B. R. Johnson, S. G. Glogover, and J. L. Kinsey, J. Chem. Phys. **101**, 1914 (1994).
[87] H. Wenz, W. Demtröder, and J. M. Flaud, J. Mol. Spectrosc. **209**, 267 (2001).
[88] R. Jost, M. Joyeux, S. Skokov, and J. M. Bowman, J. Chem. Phys. **111**, 6807 (1999).
[89] J. Weiß, J. Hauschildt, S. Yu Grebenshchiov, R. Düren, R. Schinke, J. Koput, S. Stamatiadis, and S. C. Farantos, J. Chem. Phys. **112**, 77 (2000).
[90] H. Ishikawa, R. W. Field, S. C. Farantos, M. Joyeux, J. Koput, C. Beck, and R. Schinke, Annu. Rev. Phys. Chem. **50**, 443 (1999).
[91] A. Chichery, A. Barbe, V. G. Tyuterev, and M. T. Bourgeois, J. Mol. Spectrosc. **206**, 1 (2001).
[92] A. Perrin, J.-M. Flaud, A. Valentin, C. Camy-Peyret, N. Gbaguidi, and A. N'Gom, J. Mol. Struct. **517–518**, 157 (2000).
[93] A. Perrin, J.-M. Flaud, A. Valentin, C. Camy-Peyret, and N. Gbaguidi, J. Mol. Spectrosc. **200**, 248 (2000).
[94] A. Perrin, J.-M. Flaud, F. Keller, M. A. H. Smith, C. P. Rinsland, V. Malathy Devi, D. C. Benner, T. M. Stephen, and A. Goldman, J. Mol. Spectrosc. **207**, 54 (2001).
[95] A. Chichery, A. Barbe, V. G. Tyuterev, and S. Tashkun, J. Mol. Spectrosc. **205**, 347 (2001).
[96] T. G. Slanger and P. C. Cosby, J. Phys. Chem. **92**, 267 (1988).
[97] J. M. Gomez Llorente and E. Pollak, Annu. Rev. Phys. Chem. **43**, 91 (1992).
[98] H. S. Taylor, in *Molecular Dynamics and Spectroscopy by Stimulated Emission Pumping*, edited by H.-L. Dai and R. W. Field (World Scientific, Singapore, 1995).
[99] S. C. Farantos, Int. Rev. Phys. Chem. **15**, 345 (1996).
[100] S. C. Farantos, Comput. Phys. Commun. **108**, 240 (1998).
[101] M. E. Kellman, Annu. Rev. Phys. Chem. **46**, 395 (1995).
[102] R. Prosmiti, S. C. Farantos, and H. Guo, Chem. Phys. Lett. **311**, 241 (1999).